METHOD DEVELOPMENT FOR THE DETERMINATION OF SURFACE ZETA POTENTIAL OF SILVER COATED NYLON SUBSTRATES

A thesis presented to the faculty of the Graduate School of
Western Carolina University in partial fulfillment of the
requirements for the degree of Master of Science in Chemistry.

By

Jace Brennan Walk

Director: Dr. Channa R. De Silva
Associate Professor of Chemistry
Department of Chemistry and Physics

Committee Members:
Dr. Rangika S. Hikkaduwa Koralege, Chemistry

November 2021

ACKNOWLEDGEMENTS

I would like to thank my committee members and my project director for their assistance, encouragement and patience. In particular, Dr. David D. Evanoff, Jr., has worked very hard to assist me on this project at every turn going above and beyond, even after he left WCU. I would also like to thank the WCU department of physics and chemistry for allowing me access to the tools needed for this project as well as supporting me in its completion.

I would also like to extend my thanks to Paul Venturo, a good friend who listened to me complain about my struggles over the course of this project, but always helped whenever he could. Lastly, I would like to thank my family for their continued support and encouragement.

TABLE OF CONTENTS

LIST OF TABLES

LIST OF FIGURES

LIST OF ABBREVIATIONS

ZP: zeta potential
SZP: surface zeta potential
AZP: apparent zeta potential
EDL: electrical double layer
NP: nanoparticles
SERS: surface-enhanced Raman spectroscopy
UV-Vis: ultraviolet-visible spectroscopy
ICP-OES: inductively coupled plasma-optical emission spectroscopy

ABSTRACT

METHOD DEVELOPMENT FOR THE DETERMINATION OF SURFACE ZETA POTENTIAL OF SILVER COATED NYLON SUBSTRATES

Jace Brennan Walk, M.S.

Western Carolina University (November 2021)

Director: Dr. Channa R. De Silva, Ph.D.

Surface zeta potential (SZP) is an electro kinetic property of surfaces that is a result of the electrical double layer (EDL) that forms when a surface possessing a surface charge is dispersed in a bulk material.[1] The EDL is made up of the stern layer containing tightly packed ions of the opposite charge of the surface, that extends from the surface to the diffuse layer, and the diffuse layer which contains ions of mixed charge that extends from the end of the stern layer to the slipping plane.The slipping plane is the interface between the particle or surface and the dispersant, the potential at this interface is the zeta potential (ZP).[1] The goal of this project is to develop a method for measuring the surface zeta potential of silver coated nylon substrates. The effects of the measurement process on the surfaces were investigated and the SZP was measured at pH 5, 7 and 9.2 to see how varying pH affects SZP measurements. The measurement process was found to cause a rearrangement of the silver surface, although the mechanism of this rearrangement was not investigated. The method using in this project in combination with the dip cell arrangement purposed by Corbett, *et al.*, resulted in quantifiable data for the determination of the SZP of silver coated nylon substrates under standard conditions using the tracer suspension provided by Malvern and at pH 5, 7 and 9.2 using a silica

tracer suspension. There are still more ways in which this method can be expanded upon, but this project has set the foundation in place to move forward with the measurement of the SZP of sliver coated nylon substrates. Hopefully this foundation will lead to better understanding of SZP of silver coated nylon substrates and with it a better understanding of how things interact with the surface. This understanding would allow for the optimization of surface chemistry interactions, such as the interaction of human bodily fluid with the silver coated nylon evidence swabs being developed by the Evanoff research group for the one-step, non-destructive Surface-enhanced Raman spectroscopy (SERS) analysis of human bodily fluids found in sexual assault cases.

CHAPTER 1. BACKGROUND

1.1 Introduction to Zeta Potential

Zeta Potential (ZP) is the potential difference between the electrical double layer (EDL) , which forms when a surface with a surface charge is dispersed in a liquid with an ionic strength, and the bulk material in which the surface is dispersed.[2] Zeta potential is also referred to as electrokinetic potential and can be applied to macro surfaces as well as micro/nano surfaces, in which case it is referred to as surface zeta potential (SZP). This phenomenon is caused by the formation of the electrical double layer, shown in Figure 1, which forms at the solid/liquid interface and is the result of the surface's charge influencing the arrangement of the ions or molecules within the bulk material with which it is dispersed.

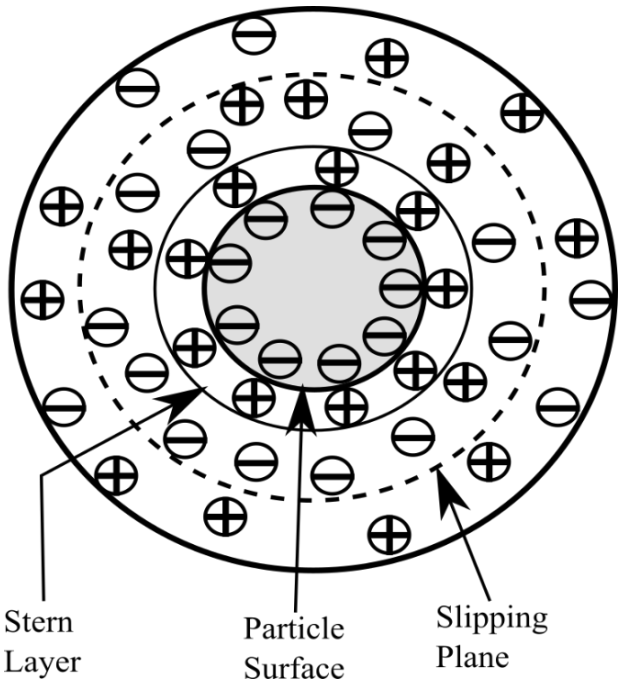

Figure 1. Diagram of the electric double layer broken down into its components, the particle surface, stern layer and slipping plane.

The EDL theory states that the ions will arrange themselves to offset the surface charge of the surface, this leads to the formation of a double layer.[3] The first layer consist of bulk ions or molecules with opposite charge, compared to the surface, which form a tight layer close to the surface called the Stern layer.[2,3] The second layer of the EDL is a diffuse layer composed of ions or molecules with mixed charge, caused by the influence of the surface's charge weakening the further it extends from the stern layer to the slipping plane.[2] The composition of this diffuse layer is dynamic and varies based on the influence of various factors such as pH, ionic strength, concentration etc.[2,3] The slipping plane is the interface between the dispersant structured by the particle or macro surface's surface charge and the bulk dispersant which is no longer affected by the surface charge of the particle or macro surface; it is the potential at this plane that is known as zeta potential.[2] The EDL arrangement at the particle and macro surface is shown in

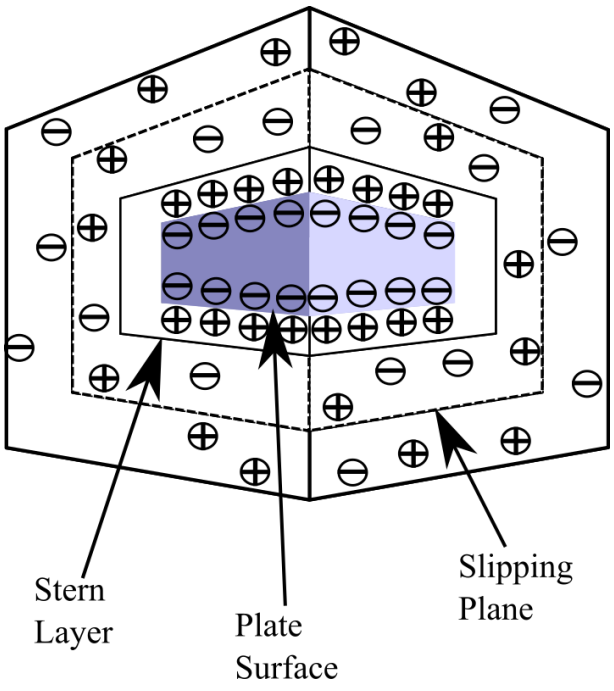

Figure 2.

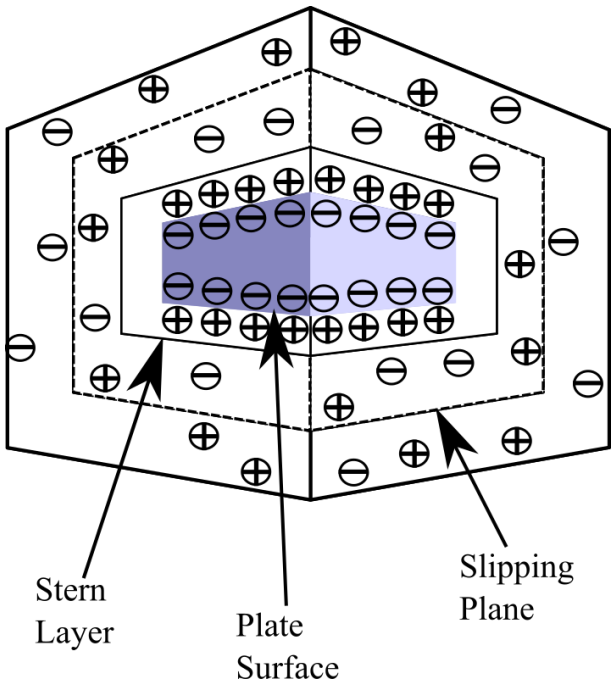

Figure 2. The EDL arrangement a macro surface, in this case a plate, broken down into its components, the particle surface, stern layer and slipping plane.

1.2 Measuring Zeta Potential

Measuring ZP cannot be done directly and therefore is deduced from the electrophoretic mobility of the particles when an electric field is applied.[2] The particles are influenced and moved by the applied electric field and scatter the light from a laser as they move. The difference in the laser source frequency and the apparent frequency of the scattered light are proportional to the particle speed as it moves through the dispersing medium, this is known as Doppler shift. The particle velocity (V) is then deduced from the Doppler shift, before being used to calculate the electrophoretic mobility (μ_e) as seen in Equation (1) where E is the electric field strength (Volt/cm).The electrophoretic mobility is then used in the Henry's equation to calculate the ZP (ζ) of the particles shown in Equation (2) where ε_r is the dielectric constant, ε_0 is the permittivity of vacuum, $f(Ka)$ is Henry's function and η is viscosity at the experimental temperature.[2]

$$\mu_e = \frac{V}{E} \tag{1}$$

$$\mu_e = \frac{2\varepsilon_r \varepsilon_0 \zeta f(\mathrm{Ka})}{3\eta} \tag{2}$$

If the particle radius is greater by comparison than the thickness of the EDL due to the aqueous solution having a high salt concentration greater than or equal to 10^{-2} molar (M); then the f(Ka) becomes 1.5 and the Henry's equation changes into the Helmholtz-Smoluchowski equation (Equation (3)).[2]

$$\mu_e = \frac{\varepsilon_r \varepsilon_0 \zeta}{\eta} \tag{3}$$

Zeta potential is measured indirectly, as explained above, from the electrophoretic movement of the particles in an electric field.[2] The method detailed above and the method used in this research is the light doppler electrophoresis method.[4] This method uses a laser to measure the electrophoretic movement meaning the suspension has to be optically transparent. This is usually achieved by diluting the sample until optical transparence is reached, however, this introduces potential changes in the zeta potential as a result of the dilution causing a change in ionic strength.[4] A second method uses sound waves in order to measure the electrophoretic movement of the particles, this method is called the electroacoustic method.[5] The particles in the suspension will move in response to an alternating voltage being applied, this movement produces sound waves. This effect was named the electrokinetic sonic amplitude (ESA). This

method has the benefit of not needing optically transparent suspensions and can therefore be used without having to dilute the sample. [5]

1.3 Methods to Measure Surface Zeta Potential

There are multiple ways to measure the ZP of a macro surface, i.e., the surface zeta potential. These ways include streaming potential, capillary flow and the use of a dip cell arrangement.[1] The streaming potential method uses an electrolyte that is flowed past the surface being tested and measures the streaming potential (ΔE_{str}) as the electrolyte flows past the surface.[1] The streaming potential is the potential difference when the current is at zero.[6] This potential difference is caused by the pressure gradient present across a charged capillary and produces a convection flow of charge.[6] By exerting a force on the EDL in the solution that had built up near the charged surface, a streaming potential is generated.[6] The streaming potential is measured using a multimeter and then, using Equation (4) where ε is the permittivity of medium used, η is viscosity, λ_0 is the conductivity of bulk material, λ_s is the conductivity of the surface, r is the capillary radius and ΔP is the applied pressure difference; the SZP (ζ) can be calculated.[6]

$$\Delta E_{str} = \frac{\varepsilon \zeta \Delta P}{\eta \left(\lambda_0 + \frac{2\lambda_s}{r} \right)} \tag{4}$$

This method requires the sample to be sealed to the sample chamber in a way that allows for high pressure.[1]

The capillary flow method requires a capillary where the opposing walls of the capillary are the surface being tested.[1] This method places the capillary, which is filled with dispersed tracer particles, into an electrical field in order to measure the electroosmotic flow of the particles through the capillary. The electroosmotic flow is measured using a fluorescent dye

which is then excited with a laser before being tracked with a florescence detector.[7] The electroosmotic flow of the tracer particles in the capillary is then compared to that of the particle dispersions that were not exposed to the electric field.[1] This data can then be used to back calculate the surface zeta potential of the samples on the capillary walls. The capillary flow method has drawbacks, it requires proper sealing of the samples to the optical parts of the capillary which limits its use to samples that can be coated onto the walls of the capillary. The tracer particles tend to sediment causing the surface potential of the surface they collect on to fluctuate.

In response to the challenges associated with measurements of SZP by these previous methods, the dip cell arrangement method was reported by Corbett, *et al*.[1] This method uses a dip cell, which is composed of a 4 millimeter (mm) by 5 mm sample stage that is positioned between two small electrodes, as shown in Figure 3.[1]

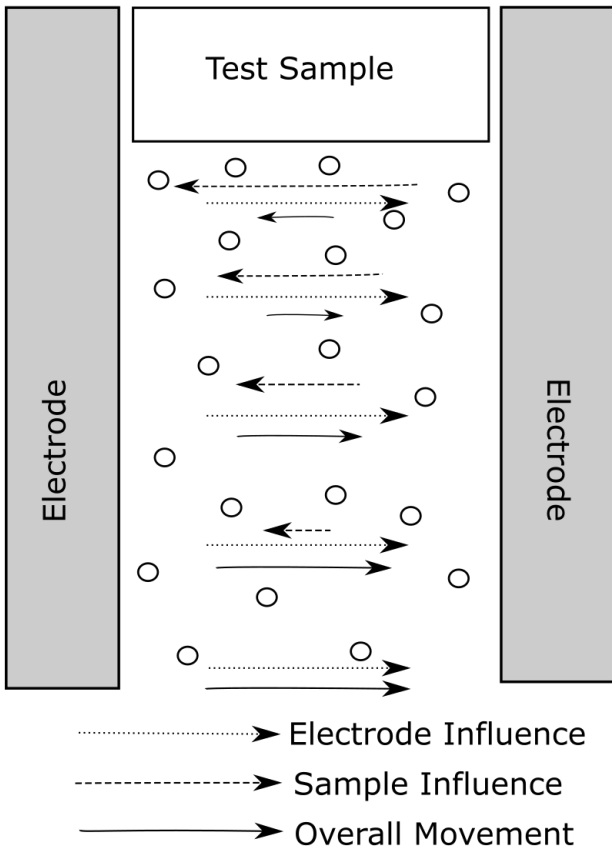

Figure 3. Sample and electrode set up for zeta potential measurement using a dip cell with electrode influence, sample influence and overall movement included.

This design allows for the sample to be placed on the sample plate without the need for pressure sealing, although an adhesive is needed, before the dip cell arrangement is placed into a cuvette containing the tracer particles of choice.[1] The particles that are the farthest away from the sample are only influenced by the electric field generated by the electrodes and therefore move with the electric field, producing a ZP measurement of the tracer particles. However, particles that happen to be closer to the sample surface are influenced not only by the electrode but also by the surface charge of the test sample, and the overall particle movement is a function of both of those influences. In Figure 3, this relationship is depicted in which the influence of the sample surface charge is strongest at the sample surface and decreases farther from the surface, as indicated by

the decreasing size of the arrows indicating sample influence. As can be seen in the figure, this "sample influence" counteracts the "electrode influence", i.e., the electric field generated by the electrodes that is constant with respect to the distance from the sample surface. The "overall movement" of the tracer particles is a function of both of these counteracting influences and produces an apparent zeta potential (APZ) of the tracer particles that varies as a function of distance from the sample surface. The "dip cell technique" described above was designed to makes use of the measurement geometry of a standard dynamic light scattering/zeta instrument and the dip cell fits in a standard cuvette. Typically, DLS/zeta instruments have a stationary laser and detector. While optics can adjust the depth into the cuvette from which scattered light is collected, the laser enters the cuvette at a specific height from the cuvette base. In order to collect data on tracer particle motion from various distances from the sample surface, the sample plate is mounted onto a micrometer screw that is perpendicular to the laser propagation vector for precise control of distance between the sample face and laser beam. By moving the sample plate closer to the plane through which the laser propagates, the data on mobility of the tracer particles influenced by the sample can be collected. While moving the sample away from the plane of the laser allows data from the "non-influenced" tracer particles to be collected. The issue of particle sedimentation is nullified due to the sample facing down in the cuvette, causing the particles to fall away from the sample and towards the bottom of the cuvette if sedimentation occurs.[1] In this method, the electrophoretic movement of the particles in the electric field produced by the electrodes is measured through light scattering off of the particles.[8] By measuring the electro-osmotic flow caused by the surface charge of the sample interfering with the electrophoretic movement of a region of particles and continuing to measure that region as the surface is moved away at specific intervals, until the electroosmotic flow no longer affects their electrophoretic

movement, the surface zeta potential of the surface can be determined.[8] The dip cell arrangement also allows for the measurement of expensive, fragile and/or small samples, due to the small size of the sample plate, the lack of pressurization and capillaries.[1]

1.4 Importance of Zeta Potential

Applications of zeta potential have been studied in various fields. The study of nanoparticles is one field where zeta potential is used regularly. A study by Sun *et al.*, investigated the effect that zeta potential and particle size had on silicon dioxide ($SiO_{2)}$ nanosphere stability, which they were using as carriers for ultrasound imaging contrast dyes.[9] Their goal was to synthesize SiO_2 nanoparticles (NP) that could achieve high resolution imaging in areas outside of the blood vessel. To achieve this goal, they needed NP with the right size and controllable zeta potential, but in order to do this they needed to understand how those two parameters effected that stability of the NP. The particles were synthesized by performing hydrolysis on and condensing tetraethyl orthosilicate (TEOS) in a mixture containing ethanol, ammonia and water.[9] The zeta potential of these particles was investigated as a parameter for determining the stability of the particle, as a zeta potential value of greater than + 30 mV or less than – 30 mV indicates a stable suspension. The zeta potential of the particles was found to be favorably negative, although it was found to become less negative when the particle size of the unmodified SiO_2 increases. This decrease in zeta potential was most evident with the SiO_2 NP of approximately 800 nanometers (nm) and was attributed to morphology changes, irregular sphere shape and small particle formation, observed using a transmission electron microscope (TEM).[9] The SiO_2 NP were then modified with the addition of an amino group, resulting in a the ZP of the different particle sizes increasing most notably the 400 nm particles increasing from -37.7 mV to -45.5 mV. This increase in zeta potential is an indication of the SiO_2 NP having a high

degree of stability after undergoing the amino modification. Their results found that the 400 nm SiO_2 NP had good stability and the appropriate size to pass through the endothelial barriers found in tumors, but not in normal tissue allowing for the delivery of the imaging agents beyond just the blood vessels.[9]

In the field of environmental science, the effects of zeta potential on the adsorption of heavy metals have been investigated. A study by He *et al.*, looked at how the surface zeta potential of hydrous manganese dioxide (HMO) influenced its ability to adsorb heavy metal ions.[10] The adsorption of the heavy metal ions Pb(II), Cd(II) and Ni(II) were investigated.[10] The HMO was found to have a large adsorption capacity with more negative zeta potential values, obtained by decreasing the ratio of Mn^{2+} to MnO_4^- in the synthesis of the HMO.[10] The zeta potential was then observed to increase as the heavy metal ions adsorbed.[10] The zeta potential was measured after five rounds of heavy metal adsorption and regeneration of the adsorbent with 50% $KMnO_4$, the zeta potential had decreased to -50.6 mV from -52.8 mV with the removal efficiency of Pb(II) falling to 91% compared to the 93% of the initial HMO.[10] This study shows the HMO absorbent's surface zeta potential might be a useful parameter in determining its efficiency in removing heavy metal ions in contaminated water sources.[10]

Surface zeta potential has also been used as a tool to monitor changes in surface chemistry, specifically surface charge, when a surface undergoes chemical treatment or modification.[8] An investigation was conducted by, Vasconcelos, *et al.*, which focused on three carbon materials, amorphous carbon, hydrogenated amorphous carbon and oxidized amorphous carbon.[8] They used a DC-magnetron sputtering chamber to create carbon films and used the method described by Corbett *et al.*, to determine the surface zeta potential of the films.[8] The SZP of the thin films were investigated as a function of pH by using sulfate latex beads and aliphatic

amine latex beads as the tracer particles.[8] They found that at pH 7.4, the amorphous carbon film had SZP values -51±2 and -63±5 mV for the sulfate latex and aliphatic amine latex suspensions respectively.[8] When the pH was dropped to 4.4, the SZP was measured to be -25 mV showing that the SZP increased as the pH decreased.[8] The pH at which the amorphous carbon film reaches its isoelectric point was determined by extrapolating the data along the pH axis, resulting in an isoelectric point at pH 3.0 for the sulfate suspension and 3.7 for the amine suspension.[8] The SZP of the hydronated amorphous carbon films at 7.4 pH were -45±4 mV, however, it was difficult to determine a clear trend from SZP verses pH so calculating the isoelectric point was not attempted.[8] The oxidized amorphous carbon films showed SZP values at -61±4 mV for the sulfate latex suspension and -75±2 mV for the aliphatic amine latex suspension.[8] The isoelectric point was found by extrapolating the pH axis, resulting in an isoelectric point of less than 1.5.[8] This study shows that pH dependent measurements can be made using the Corbett, *et al.*, method and that the isoelectric point of the carbon materials in question were able to be extrapolated from the relation shown when SZP verse pH is graphed.[8]

Zeta potential has also been investigated in a similar way to the research presented in this paper. A study performed by Morga, *et al.*, looked at the stability of silver nanoparticle monolayers.[11] The stability of silver nanoparticles deposited onto a mica substrate that had been modified with poly(allylamine hydrochloride) (PAH) was determined using *in situ* streaming potential methods. The study found that by using the ZP of the PAH in bulk and the ZP of the bare mica the ZP of the PAH covered substrate could be calculated by Equation (5)(5)(5)(5)(5)(5)(5)(5)

$$\zeta(\Theta) = F_i(\Theta)\zeta_i + F_p(\Theta)\zeta_p \quad (5)$$

where the zeta potential of the polyelectrolyte covered surface is $\zeta(\Theta)$, ζ_i is the ZP of the bare mica substrate, ζ_p is the ZP of the PAH molecules in bulk, the $F_i(\Theta)$ and $F_p(\Theta)$ terms represent the dimensionless functions of coverage and the thickness of the EDL. Equation (5) shows that the ZP of the polyelectrolyte covered substrate is a weighted average derived from the ZP of the surfaces independent from one another, but with their influences weighted according to the parameters of coverage and EDL thickness. The effect of this ZP on the coverage of the deposited silver nanoparticles was then investigated. They found that the formation of the silver monolayer resulted in an abrupt decrease in the ZP when compared to the coverage (Θ_s). So for lower levels of coverage (Θ_s<0.1) the SZP would drop in excess of 10 mV, while at higher coverage levels (Θ_s>0.1) the change in ZP values became minor and when the coverage reached above 0.25 the ZP of the silver monolayer became asymptotic with values of -32 mV, -27 mV and -23 mV for ionic strength values of 10^{-3}, 10^{-2} and 0.15 M NaCl, respectively. This finding confirmed that for high coverage ranges of silver nanoparticles, the limiting ZP approaches $1/\sqrt{2} = 0.71$ of the zeta potential of the bulk silver nanoparticles. This was then repeated for the pH values of 5.5 and 9 resulting in asymptotic values of -27 and -35 mV, respectively. This study used an electrokinetic model (based on Equation (5)) and through experimentation showed that the model could be used to interpret the behavior of a real nanoparticle system.[11]

1.5 Introduction to Raman and Surface Enhanced Raman Spectroscopy (SERS)

An understanding of ZP and SZP allows insight into the mechanism of certain spectroscopy techniques where the signal produced can be impacted by the physiochemical interaction between a nanostructured surface and the analyte. An example of one of these surface-enhanced spectroscopy techniques is SERS, or surface-enhanced Raman spectroscopy.

Raman spectroscopy is a vibrational spectroscopy technique that uses an incident laser beam to induce inelastic scattering from an analyte molecule.[12] There are two types of scattering that can occur, elastic scattering or inelastic scattering.[12] Elastic scattering occurs when the photons from the excitation source collide with the surface of the sample and deflect with the photon having undergone no change in energy from the collision, Rayleigh scattering is a form of elastic scattering.[12] Inelastic scattering occurs when a photon from the excitation source does undergo a transfer of energy between it and the sample during the collision.[12] Raman scattering is a form of inelastic scattering and is the type of scattering detected through Raman spectroscopy.[12] There are two types of Raman scattering, Stokes and anti-Stokes.[12] Stokes Raman scattering occurs when the photon loses energy from the collision to cause the sample molecule to move from the ground state to the vibrationally excited state, whereas anti-Stokes has the photon gaining energy from collision with a vibrationally excited molecule resulting in the molecule relaxing a lower-energy vibrational state.[12] Of the two types of Raman scattering, Stokes scattering is more common as the majority of molecules that are at rest and room temperature will be in the ground state, vibrationally.[12] Raman spectroscopy can be used to examine and identify the characteristics of individual substances from the patterns present in the spectra also known as fingerprinting. [12] Spectroscopic information from Raman spectroscopy is similar the spectroscopic information obtained from infrared absorption spectroscopy (IR); however, this information is obtained using a different excitation pathway. Due to using an excitation pathway that relies on changes in polarizability to excite the Raman bands instead of changes in dipole movements like in IR spectroscopy; Raman spectroscopy has the benefit over IR of being insensitive to water. The biggest weakness of Raman spectroscopy is the lack of sensitivity due to photons only undergoing Raman scattering once every 10^6-10^8 photons.[12]

Surface-enhanced Raman spectroscopy (SERS) is a way to enhance the scattering efficiency by a factor of up to 10^6 when compared to Raman spectroscopy.[12] SERS uses a roughened metal surface to which the analyte is on or near to enhance the Raman scattering efficiency.[12] When a photon interacts with the metal, the conduction electrons within the excitation volume, begin to oscillate collectively.[12] These oscillations, which are at the same frequency as the excitation, is called a plasmon resonance.[12] Silver and gold plasmons oscillate at frequencies that fall within the visible region and as such are highly suited for use with the visible lasers utilized for Raman spectroscopy.[12] There are two possible mechanisms that have been attributed to the plasmons ability to enhance signal.[12] The first mechanism is that a chemical bond forms between the molecule and the metallic surface nanostructure, this bond allows for the flow of electron density directly to the sample molecule from the nanostructure.[12] The second mechanism is thought to be that an electric field is created, due to plasmons being oscillations of point charges, and that this electric field both oscillates and couples to the electric field of the sample molecules. In either case, the polarizability of the analyte molecule is influenced by the close proximity of the analyte to the metal's oscillating electrons such that Raman scattering becomes much more probable [12]

SERS has been used to solve various analytical questions. In a study conducted by Jumin Hao, *et al.,* SERS was investigated as a method for the detection of arsenic (As) in water.[13] Arsenic is a metal that is toxic to humans and has been found as a contaminant in water sources in many countries such as the USA, China, Japan, etc. The authors evaluated the potential of SERS as a quick, accurate, and relatively inexpensive method for arsenic testing in the field. For the detection of arsenic, three substrates were used: two Ag nanofilms (AgNF) and an Ag nanowire (AgNW). Using Ag nanowire substrate, it was found that the characteristic peaks,

caused by the $\nu_1(A_1)$ symmetric As-O stretching mode, for the species As (V) produced SERS bands at 780 and 812 cm^{-1} for the excitation wavelengths of 785 and 532 nm, respectively. The Ag nanofilm substrate was found to have a detection limit lower than 5 parts per billion (ppb) which allows for even trace amount of arsenic to be detected. Using the same substrates, the more toxic As (III) species can also be detected and identified within the same sample as the As (V) species. This is possible due to As (III) producing SERS bands at 721 to 750 cm^{-1} compared to As (V) producing bands as 780 to 821 cm^{-1}. This was accomplished despite the two species having the same $\nu_1(A_1)$ symmetric As-O stretching mode, as SERS allows for the detection of the different chemical environments in the species. A portable Raman spectrometer was used to perform SERS analysis on 16 groundwater samples, the results were then compared to atomic fluorescence spectroscopy (AFS) results with a deviation of 26% for As (III) and 12% for As (V) between the two measurement methods. This showed that SERS techniques have the potential for practical applications in the rapid screening and monitoring of arsenic in water sources both in the field with portable Raman spectrometers and in the laboratory.[13]

Another study performed by Andrei Stefancu, *et al.,* investigated SERS for use in the medical field to analyze serum with prostate-specific antigen (PSA) in order to improve the detection of prostate cancer.[14] Using PSA screening to diagnose prostate cancer is a much debated topic as elevated levels, above 4 ng/mL, can indicate prostate cancer, but could also be caused by benign prostatic hyperplasia, prostatitis or urinary tract infections. On the other hand, even a level lower than 4 ng/mL does not guarantee that a patient does not have prostate cancer as upwards of 15% of patience with this PSA level do have prostate cancer. This can lead to easy misdiagnosis of prostate cancer and as such the team turned to a statistical model that combines the PSA data and SERS spectra for diagnosis. The team used 54 blood serum samples, 30 from

prostate cancer patients and 24 control samples from patients with benign prostatic hyperplasia. The hydroxylamine hydrochloride reaction method was used to synthesize SERS-active silver nanoparticles, 2 mL of the silver colloid was then concentrated via centrifuge for 15 minutes at 5800 g and resuspended in 50 μL of water. Microscope slides then had a mixture of 1 μL of serum and 9 μL of the concentrated silver NP colloid deposited onto it before being covered with aluminum foil and allowed 20 minutes to dry for each serum sample. The rim of the samples on the microscope slides were analyzed using SERS spectroscopy across the 606-1715 cm^{-1} range with two measurements being averaged for each sample. The Unscrambler (X version, CAMO Software, Oslo, Norway) and GraphPad Prism (Version 6.0, GraphPad Software) software packages were used to analyze the data. This data analysis involved removing the background using linear baseline correction, then normalizing the mean and performing principal component analysis-linear discriminant analysis (PCA-LDA) with the first 15 principal components (PC's). The PSA level data was divided by their median vale in order to normalize the data, this data was then appended to the SERS spectral data before performing the PCA-LDA on the resulting matrix. Other tests on this data includes unpaired t-test, Mann-Whitney nonparametric tests, the D'Argostino & Pearson omnibus normality tests and receiver operating characteristic (ROC) curve analysis. By combining the PSA level data with the SERS data, the accuracy of identifying between patients with prostate cancer and controls was 94% as opposed to the 90% for the spectral analysis and the 70.4% for the PSA level analysis when performed individually.[14] This study demonstrates how SERS analysis has also been adopted to answer analytical questions in the medical field.

SERS is also being used in the Evanoff research group to answer forensics questions. Nylon evidence swabs are having nanostructured metallic surfaces grown onto them to obtain a

surface for SERS enhancement.[15] The suitability of these SERS-active swabs is being evaluated for the collection of human bodily fluids in sexual assault cases. These swabs will allow for the collection of human bodily fluids directly onto a SERS-enhanced surface that can then be used to perform a non-destructive, confirmatory analysis to identify the bodily fluids present on the swab. This one-step, non-destructive test would be a huge improvement to the current testing procedure, which requires each bodily fluid to be tested for separately and destroys the sample used. Likewise, the SERS-active swabs have been shown to not interfere with the extraction and genotyping of DNA from the fluids.[16]

1.6 SERS and Zeta Potential

Zeta potential has also been investigated by Alverez-Puebla, *et al.,* as a parameter that affects surface enhanced Raman scattering (SERS). [17] SERS is a technique that allows for extremely sensitive chemical analysis and the study of interfaces.[17] SERS can provide a molecular "fingerprint" by using the highly informative content obtained from vibrational spectroscopy.[17] SERS can also detect down to the level of a single molecule.[17] However, a prerequisite for strong surface enhancement of the Raman signal is the adsorption of the analyte molecules onto the metal colloid particles.[17] The adsorption of the analyte onto the particles is affected by the surface charge of the particles and even small changes in the surface charge can significantly affect the surface enhancement of the Raman signal.[17] Due to surface charge having a large effect on SERS measurements, Alverez-Puebla, *et al.,* set out to establish a direct connection between the ZP and the SERS intensity of common colloidal suspensions in order to determine the role of NP surface charge and by extension ZP in SERS.[17] Salicylic acid, pyridine and 2-naphthalenethiol were added, in a ratio of 10 μL per milliliter of pH-adjusted colloid, to three colloidal metal suspensions, one silver borohydride, one silver citrate and one gold citrate,

to prepare the SERS samples.[17] SERS spectra was then obtained using a Reinshaw Invia system with a Peltier cooled CCD and utilizing a Leica microscope. The spectra were collected using the Reinshaw's continuous collection mode with a laser excitation at 633 nm, a 10 second accumulation time and the coaddition of five spectra. The silver borohydride colloidal suspensions had a ZP range from 6.5 mV at a pH of 2 to -56 mV at a pH of 11. From pH 2 to pH 6 the colloid collapsed and underwent partial aggregation, this was due to the magnitude of the ZP not reaching above the typical stability threshold of ±30 mV until pH values higher than 6.[17] This in turn corresponded to the surface plasmon absorption intensity decreasing across the pH 2 to pH 6 range with the extinction intensity stabilizing across the pH 7 to pH 11 range.[17] The silver citrate colloids were found to be stable across the pH range of 2 to 12.[17] The ZP at pH 2 of -20 mV before sharply decreasing to -48 mV at pH 6, then slowly approaching the ZP of -52 mV at pH 10 and finally remaining constant from pH 10 to 12.[17] The pH changes were observed to only influence the surface charge of the silver citrate with the maximum surface plasmon absorbance remained at 442 nm across the pH range.[17] The gold citrate colloidal suspensions had the most negative ZP values out of the three suspensions investigated as well as having highest stability.[17] The gold citrate suspension's plasmon absorption wavelength showed no shifts from pH 2 to 12.[17] They concluded that the average intensities of the SERS spectra from the colloid suspensions are strongly related to the pH of the solution and the ZP. The surface charge also influences the aggregation of the particles as well as the electrostatic interactions between the particles and the analytes allowing for optimization of the SERS measurement conditions.[17] The study found that the SERS enhancement is generally strongest when the NP suspensions are stable and the electro static repulsion is minimized between the particles and analytes, as indicated by the ZP.[17] This conclusion makes sense as the analyte needs to be able to approach

the surface in order for SERS enhancement to occur. However, does the analyte have to make it to the loosely organized slipping plane, does it have to make it to the tightly packed stern layer or does the analyte have push through the stern layer and bind to the surface itself to maximize this enhancement factor? These questions require a greater understanding SZP and how it interacts with SERS to answer.

1.7 Research Goals

The purpose of this research was to develop a method for measuring the surface zeta potential of nanocoated material, specifically silver on polymeric substrates. This research was performed to determine (1) if the measurement parameters cause damage or degradation to the nanocomposite, (2) the effects of the pH of the system on the surface zeta potential of the nanocoated material and (3) to create a method that could become the foundation for the measurement of surface zeta potential of other silver coated substrates; such as the silver coated nylon evidence swabs being developed in the Evanoff research group for SERS analysis of bodily fluids.

The first goal was to determine if the zeta potential transfer standard provided by Malvern has any interaction with the nanocoated material, silver in the case of this research, such as degradation or removal of the nanocoated layer. This was quantified using sample solutions that have been exposed to the tracer material as well as solutions produced from samples that have not been exposed to the tracer material. The amount of the nanocoated material was quantified using the Inductively Coupled Plasma-Optical Emission Spectroscopy (ICP-OES).

The second goal was to vary the pH of the solution of tracer material. This was done to see how pH affects the surface zeta potential of the nano coated surface as the tracer material provided by Malvern is at a pH of 9.2. By doing this, data about how the environmental pH

around the nanocoated surface affects the surface zeta potential could be obtained. For this goal, the pH values to be investigated were chosen to be four, seven and ten, which allowed for reasonable characterization of how the surface zeta potential was affected by acidic, neutral and basic environments.

The third goal was for the method developed by this research to serve as a foundation for further research into surface zeta potential measurements of other nanocoated material, including using non-planar samples, such as the silver coated nylon evidence swabs that are also being developed in the Evanoff research group.

The surface zeta potential was measured over a range of pH values using a Malvern Zetasizer Nano ZS, the dip cell arrangement method proposed by Corbett, *et al*., and dynamic light scattering.[1] These measurements were accomplished by creating silver coated nylon substrates using sheets of virgin nylon that were cut to fit the dip cell sample plate, before having silver metal deposited onto the substrates via a thermal evaporator.

CHAPTER 2. EXPERIMENTAL

2.1 Materials

The dip cell arrangement kit, catalog number ZEN1020, and Zeta Potential Transfer Standard, part number DTS1235, were acquired from Malvern Pananalytical, Inc. Cyanoacrylate, Super Glue Gel by Scotch for securing samples to the plate holder. Silver nanoparticles were prepared according to the method described in the paper by Evanoff, *et al.*, using Ag_2O (99.95%) acquired from Alfa Aesar and Ultracarrier grade H_2 acquired from Airgas.[18] Silica nanospheres with a particle diameter of 293 ± 14 nm at a concentration of 3.5 x 10^{11} particles per mL dispersed in Milli-Q water were acquired from nanoComposix. Nylon sheet 1.6 mm thick was obtained from Alfa Aesar. Nitric acid, for ICP sample preparation and 99.9% silver nitrate for ICP standard preparation were obtained from Fisher Scientific. Sodium citrate dihydrate, citric acid, dipotassium phosphate, potassium dihydrogen phosphate, sodium bicarbonate and anhydrous sodium carbonate, obtained from Fisher Scientific, were used to prepare buffer solutions. 18.2 MΩ water from Barnstead Nanopure. Silver pellets (99.99 %) for thermal evaporator were obtained from Kurt J. Lesker Company. Poly (4-vinyl pyridine) (PVP), average molecular weight of 60,000, for silver coated slide preparation was obtained from Sigma Aldrich.

2.2 Sample Prep

2.2.1 Zeta Potential Samples

Substrates measuring approximately 4 millimeters (mm) by 4 mm were cut from a sheet of virgin nylon. These substrates were then placed into a custom holder cut from the same sheet of virgin nylon. This holder was then placed inside a Denton Vacuum model DV-502A thermal evaporator where silver was evaporated onto the substrate. The chamber was evacuated to below

4.2 x 10^{-6} torr, the deposition rate was held at 1 angstrom per second (Å/s) and resulted in a silver layer with an average thickness of 35 nanometers (nm) as measured by a quartz crystal microbalance collocated in the evaporation chamber with the nylon substrates. Substrates, other than those reserved for control group samples, were rinsed with ultrapure water to remove any potentially unbound silver from the surface and dried with a stream of argon. These silver coated substrates were then glued to a dip cell plate using cyanoacrylate, Scotch brand Super Glue Gel superglue before being adjusted with a scalpel to fit between the electrodes of the dip cell.

2.2.2 Silver Coated Glass Slides

Glass slides were scored and broken into smaller slides using a glass scoring pen. These smaller slides were washed with ultrapure water before being dried with argon gas. The slides where then submerged in a solution of 2% by mass poly (4-vinyl pyridine) (PVP) in ethanol inside individual dram vials and placed in a vial rotator overnight. The slides were then removed, dip washed in ethanol first and then dip washed in ultrapure water before being dried with argon gas. The slides were then placed in individual dram vials containing a silver nanoparticle suspension and placed into a vial rotator overnight. The slides were removed, washed again with ultrapure water by dipping and dried again with argon gas.

2.2.3 Inductively Coupled Plasma Optical Emission Spectroscopy (ICP-OES) Samples

Samples to be analyzed using ICP-OES were first removed from the dip cell plate using a scalpel. The samples were then stripped of the silver layer using approximately 1 milliliter (mL) of concentrated nitric acid. The silver/acid samples were then diluted to 10% nitric acid by adding 9 mL of ultrapure water diluting to a final volume of 10 mL. A 200 parts per million (ppm) stock was made using silver nitrate ($AgNO_3$). Standards of 10, 5, 2.5, 1, 0.5, 0.25 and 0.05 ppm were prepared from the stock by performing serial dilution with 10% nitric acid.

2.2.4 pH Trial Tracer Suspensions

Silica nanoparticles, measuring 293 ± 14 nm, were used to make 15 mL tracer suspensions at the desired pH values. The silica particles were added dropwise to a 14.6 mL volume of pH buffer, while stirring, until a final volume of 15 mL was obtained. The pH 5 buffer was prepared by mixing 848 mg of sodium citrate dihydrate, 406 mg of citric acid and 500.0 mL of 18.2 MΩ water. The pH 7 buffer was prepared by mixing 467 mg of dipotassium phosphate, 315 mg of potassium dihydrogen phosphate and 500.0 mL of 18.2 MΩ water. The pH 9.2 buffer was prepared by mixing 382 mg of sodium bicarbonate, 48 mg of anhydrous sodium carbonate and 500.0 mL of 18.2 Mohm water. The suspensions were stirred for an hour to ensure that the particles were distributed throughout the solution without them aggregating.

2.3 Instrumentation

All ZP and SZP measurements were made using a Malvern Zetasizer Nano ZS, ICP-OES data was collected using a Perkin Elmer Optima 4100DV ICP-OES and UV-visible extinction spectra were collected using an Agilent 8453 UV-visible diode array spectrometer.

2.4 Method

2.4.1 UV-Vis (Ultraviolet-Visible Spectroscopy) of Silver Coated Slides

Four silver-nanoparticle-coated glass slides described in section 2.2.2 were measured using UV-Vis spectrometry. Three of the slides were place in cuvettes with the Malvern zeta potential transfer standard, which is the tracer particle suspension that allows for the measurement of surface zeta potential, while one slide was placed in a cuvette with ultrapure water to act as a control. Each slide sat in the cuvettes until a predetermined amount of time had passed before being removed and placed into a cuvette of ultrapure water (ultrapure water was

replaced, and the cuvette washed between readings) to be analyzed by the UV-Vis. For this experiment the times used were 5 minutes, 1 hour, 2 hours, 3 hours, 4 hours and 5 hours.

2.4.2 ICP-OES of Silver Coated Substrates Number of Runs Trial

The 15 samples described in section 2.2.3 were used with ten percent nitric acid as the blank. The wavelengths used for analysis were, 243.778 nm, 328.068 nm and 338.289 nm. Three replicates were used for each sample.

2.4.3 Zeta Potential Using Dip Cell Arrangement

Sample plates were secured to the dip cell arrangement using the included screwdriver and screw. The sample plate was then coarse adjusted using the course adjustment apparatus included with the dip cell by turning the adjustment knob on the dip cell. A plastic cuvette was then rinsed with ultrapure water and filled with 1.5 mL of tracer material prior to the dip cell arrangement being inserted into the cuvette. This assembly was then inserted into the Malvern Zetasizer Nano ZS and the substrate to be measured was moved farther down into the cuvette by manual, clockwise $1/8^{th}$-turns of the fine adjustment knob at the top of the SZP dip cell assembly. This was done until the plate blocks the laser, as indicated by the count rate meter accessible in the Malvern ZetaSizer software, then the plate is turned back $1/8^{th}$ of a turn to reveal the laser again marking the position as the 0-distance point. The equilibration time was set to 120 seconds with a 60 second pause between runs. The sample is then displaced by 125 µm counter-clockwise from the 0-distance point obtained after the adjustment step. The sample is then moved in 125µm increments until it reached 625 µm. A measurement is made at each position, and then a final measurement is made at 1000 µm. This process was repeated for each sample and each run.

2.5 Data Analysis

All data was gathered from the instruments in the form of a Comma Separated Values (CSV) document and then analyzed using Microsoft Excel. Microsoft Excel was used to perform, linear regression analysis, ANOVA analysis, F tests and T tests. Statagraphics 19 was used to perform comparison of linear regression analysis.

2.5.1 Tracer Particle Zeta Potential

The first step in this research was to determine if the method being used could confirm the ZP of the tracer particles provided by Malvern. The Malvern zeta potential transfer standard and the silica tracer suspension were measured and compared at pH 9.2, which was the pH of the zeta potential transfer standard provided by Malvern. This was done using the foldable capillary zeta cell, product number DTS1070.

2.5.2 Surface Zeta Potential of Bare Nylon

The second step in this research was to determine the surface zeta potential of the bare nylon substrate. The same steps of attaching the sample and performing the measurements were used as outlined in the methods section. The number of runs used was 5, each of these runs were averaged together and the standard error was determined. The data was then graphed, and linear regression was used to calculate the surface zeta potential of the bare nylon. This was done by using the apparent zeta potential measured at the 1000 µm position (ζ_{ap1000}) and intercept (INT) obtained from the linear regression analysis with Equation 6.

$$\zeta_p = INT(-1) + \zeta_{ap1000} \tag{6}$$

The intercept is multiplied by negative one as that is the amount of energy that would be needed for the tracer particles to penetrate the electrical double layer to reach the surface, so with

respect to the surface zeta potential of the surface that value would be opposite in magnitude. Equation 6 was used to calculate the surface zeta potential in all trial performed.

2.5.3 UV-Vis Analysis of Silver Coated Slides

One concern when devising the method for analyzing the surface zeta potential of the silver coated substrate, was the effect the tracer material would have on the silver surface. In order to test this before proceeding to the coated nylon substrate, the glass slides prepared in section 2.2.2 were used to perform Ultraviolet-Visible spectroscopy (UV-Vis) using the method outlined in section 2.4.1. This experiment would show if the tracer material was causing a change in the silver surface by showing a resulting change in the UV-Vis spectrum. The three trial slides were placed into cuvettes containing the zeta tracer material, while the control slide was placed in a cuvette with ultrapure water. The slides were analyzed after 5 minutes, 1 hour, 2 hours, 3 hours, 4 hours and 5 hours had passed. They were analyzed by removing them from their cuvettes and placing them in a clean cuvette containing ultrapure water, which was changed before each analysis. A single factor ANOVA test was performed on the UV-vis data for the peak height, peak position and full width at half maximum (FWHM).

2.5.4 Preliminary Surface Zeta Potential Measurement of Silver Coated Substrate

Surface zeta potential measurements were performed on two of the samples prepared in section 2.2.1 using the method described in section 2.4.2. Each of the samples was ran four times with each of them having one run excluded as a severe outlier before data analysis. The apparent zeta potential at each displacement was averaged, the averaged apparent zeta potential for the displacements from 125 µm to 625 µm were used to calculate the slope and intercept. The intercept and the average apparent zeta potential at 1000 µm were used with Equation 6 to calculate the surface zeta potential of the silver coated substrate. This process was repeated for

each of the sample runs. The averages from the first sample runs were averaged together and linear regression and ANOVA were performed on the averages to determine the surface zeta potential and error. This process was repeated for the second sample runs.

2.5.5 Silver Coated Substrate Runs Trial

After analyzing the data for the silver coated substrates, the question of whether the number of runs influenced the surface zeta potential, or the surface arose. In order to answer this question a large batch of 15 substrates were produced as outlined in section 2.2.1. Nine of the substrates were rinsed with ultrapure water to remove excess silver. They were separated into groups of three with the first group being subjected to one run, the second group to two runs and the third to three runs. The other six samples were controls for the ICP analysis of the substrates. Three of the controls were rinsed with ultrapure water to act as "wet controls", while the other three were left as "dry controls". Each of the wet controls were exposed to the tracer material for an hour to simulate the conditions of undergoing one run in the zetasizer. This resulted in a wet control for one run, two runs and three runs. The apparent zeta potential at each displacement for each of the sample runs were averaged. The runs averages were then averaged with the other runs from that sample to obtain the sample averages. The sample averages were then averaged together to get the averages for the trial. This process was used for each of the trials. The trial averages were used to determine the slope and intercept, which in turn was used with Equation 6 to determine the surface zeta potential of each trial. Statistical analysis was then performed on this data using the free version of Statgraphics 19 to determine if the slopes and intercepts of the regression lines are statistically different from each other.

2.5.6 ICP-OES Analysis of Silver Coated Substrate Runs Trial

To determine if the number of runs a substrate is exposed to affects the substrate surface, ICP-OES analysis was necessary. The 15 samples were prepared for ICP-OES analysis using the steps outlined in section 2.2.3. Linear regression was performed on the emission intensity of the standards at 243.778 nm, 328.068 nm and 338.289 nm. Using the slope and intercept from the linear regression analysis in addition to the intensity of the sample, the concentration of the samples was determined at each of the wavelengths. The error in concentration was also calculated using the concentration of the standards, intensity and the sample intensity to calculate the concentration error.

2.5.7 pH Trials

The zeta potential transfer standard provided by Malvern was diluted using pH buffer solutions in order to obtain a tracer suspension at the desired pH. The pH values used were 9.95 and 7.10. Regression analysis was performed on the data as outlined in section 2.5.2 in order to determine the surface zeta potential and the error in the surface zeta potential.

2.5.8 Silica pH Trials

After analyzing the data from the pH Trials, it was determined that diluting the zeta potential transfer standard supplied by Malvern was not providing adequate results as the scattering intensity of the tracer particles collected by the ZetaSizer was too low. In order to perform zeta potential measurements at variable pH values, it was decided that making the tracer suspensions from the ground up would be the best option. Tracer suspensions at the pH values of 5, 7 and 9.2 were made using the method outlined in section 2.2.4. The samples were measured using the method outlined in section 2.4.2 with 3 samples per pH value undergoing 3 runs each for 9 total measurements per pH value.

CHAPTER 3. RESULTS AND DISCUSSION

3.1 Tracer Particle Zeta Potential

SZP is measured, as described in chapter 1, by measuring the electrophoretic mobility of tracer nanoparticles at different distances from the surface being analyzed. SZP is inferred by using Equation 6. One of the measurements used in Equation 6 is the uninfluenced ZP of the tracer particles, measured at 1000 µm from the test surface. The tracer particle suspension provided by Malvern consists of ca. 300 nm carboxylated polystyrene latex polymer beads suspended in aqueous media at a pH of 9.2 and an NaCl concentration of 10 mM. The buffered suspending medium with added sodium chloride ensures that the EDL of the tracer particles will be homogenous among all tracer particles in a given suspension, which improves repeatability of measurements. The tracer particles, with their certified ZP, can also be used as a standard to ensure that the instrument is properly measuring ZP. Using a folded capillary cell, the Malvern tracer particles were measured and resulted in a ZP of -42.1 ± 0.1 mV which is well within error of the -42 ± 4.2 mV reported by Malvern. While the bulk of the work presented here utilized the tracer particles provided by Malvern, hydroxyl-terminated silica nanoparticles with a diameter of 293 ± 14 nm were used for a portion of this work in which the dependance of the SZP of silver-coated nylon on pH was assessed. As described in section 2.2.4, the silica particles were diluted by suspension in buffer solutions that ranged from a pH of 5 to a pH of 9.2. This pH range was chosen in part due to the known stability of silica particle suspensions over this pH range. Likewise, the pH range somewhat mimics the range of pH of various human bodily fluids such as slightly basic seminal fluid to more acidic saliva and vaginal fluid. The ZP of the silica tracer

suspensions was measured in triplicate and then averaged to establish a baseline ZP for the desired pH values of 5, 7 and 9.2, shown in

Figure 4.

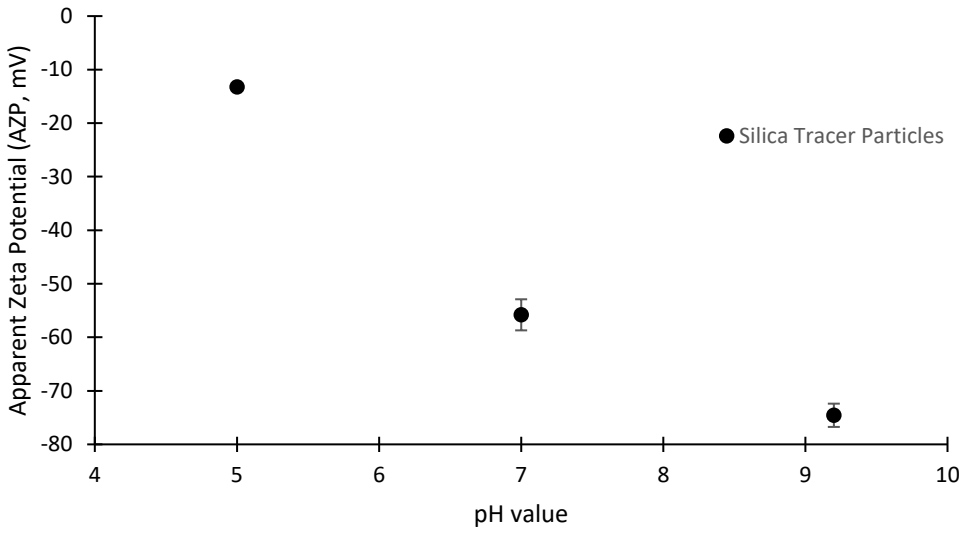

Figure 4. Averaged zeta potential for silica nanoparticles for pH 5, 7 and 9.2.

The average ZP for pH 9.2 was -75 ± 2 mV, for pH 7 it was -56 ± 3 mV and pH 5 was -13 ± 0.5 mV. This data indicated that the silica suspensions are quite stable at pH 7 and 9, while the zeta potential of the pH 5 suspensions is less than the typical ±30 mV that indicates long-term stability. The data shown in

Figure 4 is similar to data available in the literature when considering that zeta potential is not only pH dependent but is also dependent of particle size and ionic strength. For example, a study by Oh, *et al.*, found that for ca. 130 nm particles the zeta potential varied from -70 mV to -10 mV at a pH of 9.2 when the NaCl concentration was increased from 5 mM to 100 mM.[19] Likewise, Shi, *et al.*, showed that the zeta potential of silica particles ranging from 4.1 to 495.7 nm at a given pH value of 8.0 and an NaCl concentration of 0.2 mM varied by ca. 15 mV.[20]

3.2 Surface Zeta Potential of Bare Nylon Substrates

Before studying the surface zeta potential of silver-coated nylon, the SZP of bare nylon was determined. To perform this measurement, a substrate was cut from a larger nylon sheet, as described in section 2.2.1 and attached to the dip cell apparatus as described in section 2.4.3. Prior to analysis, the substrate was cleaned by sonication in ultrapure water and dried with a stream of argon gas before being placed in the tracer particle suspension. SZP data of the same nylon substrate was collected five times to better understand the 'intra-substrate' variability between measurements, i.e., the difference between multiple measurements of the same substrate. Each of these 'runs' is a collection of data collected at 5 equally spaced distances from the substrate surface, ranging from 125 µm to 625 µm and a final measurement taken at 1000 µm from the nylon surface. Data from the five runs are shown in **Error! Reference source not found.**A. Each data point is the average of 5 successive measurements and the error bars represent the standard deviation of those measurements. The dotted lines of corresponding color represent the linear line of best fit of the data set of the run. As the data at 1000 µm are not used in the linear regression calculation, that data is excluded from **Error! Reference source not found.**A.

What is apparent from **Error! Reference source not found.**A is that there is noticeable variability among the runs. For example, at 375 µm from the nylon surface, the APZ of the tracer particles varied from ca. -24 mV to -33 mV, with the later runs having more negative AZP than the earlier runs. This trend of successive runs having more negative AZP values is apparent at each measurement location. Likewise, the range over which the measurements change over successive runs is similar at each measurement position with the average difference between Run 1 and Run 5 being -9 ± 2 mV. However, the variability among the five measurements taken at 1000 µm, not shown in **Error! Reference source not found.**A, was much smaller with the

difference between Run 1 and Run 5 being -2 mV. While the cause of this trend is unknown, some potential explanations may be a change in the surface chemistry of the nylon sheet after prolonged exposure to the tracer suspension, or perhaps more likely variations in localized heat caused by repeated measurements. SZP measurements are known to be temperature dependent. Future experiments could include varying the time between runs to determine if longer times between runs better allowed temperature to re-equilibrate, leading to less variation among the runs.

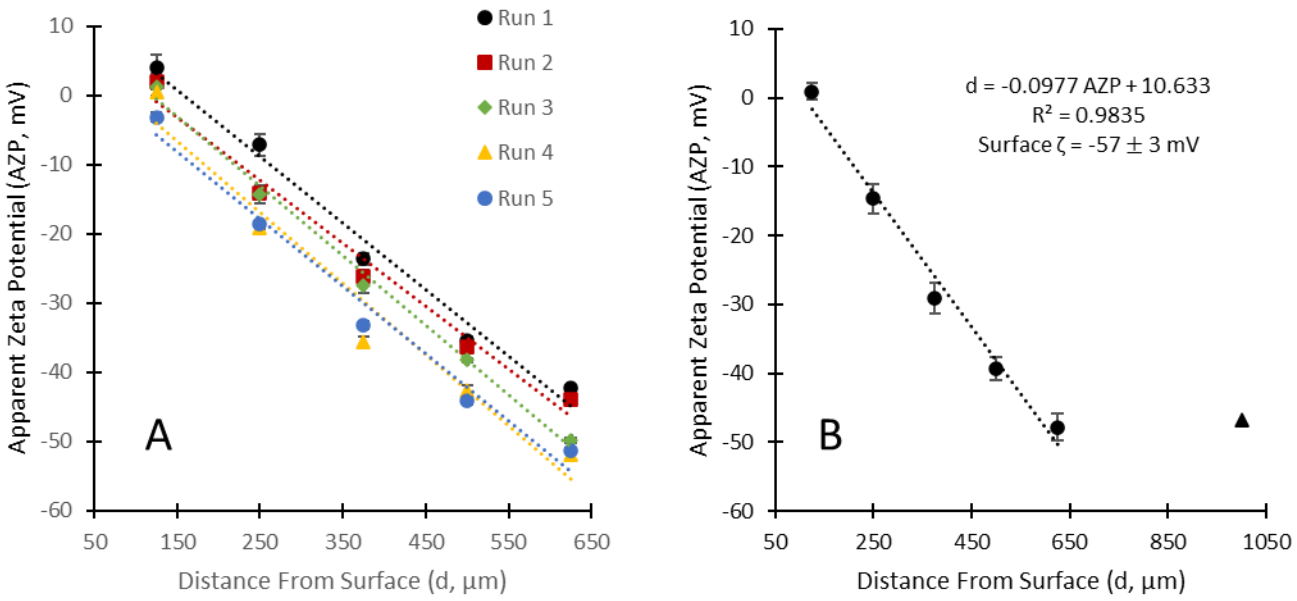

Figure 5. (A) Apparent zeta potential of the Malvern zeta potential transfer standard measured at 5 distances from a nylon substrate. The measurements were repeated 5 times (Runs 1 through 5) and the dotted lines represent the linear regression line of best fit for the data of corresponding color. The error bars represent the standard deviation of the 5 replicate measurements made at each distance. (B) Averaged SZP data for bare nylon in which circles represent averages of the data presented in Figure 5A while the triangle represents the average of the AZP data measured at 1000 µm from the nylon substrate.

To calculate a surface zeta potential for bare nylon, the AZP data at each measurement position among the 5 runs were averaged. The averaged AZP values are shown in **Error!**

Reference source not found.B, in which the error bars on each data point indicate the standard deviation among the five runs. Linear regression was performed on the data between 125 μm and 625 μm (circles in Figure 5B) to determine a slope and intercept. The intercept, along with the AZP of the uninfluenced tracer particles at a distance of 1000 μm from the nylon surface (triangle in **Error! Reference source not found.**B) were used to calculate an SZP of -57 ± 3 mV (at pH 9.2). Ripoll, *et al*. previously reported a SZP of Nylon-6,6 of -50 mV for pH 9-11.[21] Given that there may be variations in the surface treatment of the nylon used in the Ripoll measurements and those described above, these measurements are quite similar.

The data presented graphically in **Error! Reference source not found.** is also shown in **Error! Not a valid bookmark self-reference.**, in which the slope, intercept and coefficient of determination (R^2 value) from the linear regression analysis are presented along with the calculated SZP for each of the 5 runs as well as the averaged data.

Table 1. Summary of Linear Regression Analysis and calculated Surface zeta potential for each measurement of a bare Nylon substrate, as well as the averaged data. Graphical representations of this data are shown in Figure 5.

Run	**Linear Regression Analysis**			**AZP at 1000 μm**	**Surface Zeta Potential (mV)**
	Slope (mV/μm)	*Intercept (mV)*	*Coefficient of Determ. (R^2)*		
1	-0.10	15.3	0.98	-45.5	-61 ± 3
2	-0.09	10.5	0.98	-47.1	-58 ± 3
3	-0.10	12.1	0.99	-47.0	-59 ± 2
4	-0.10	8.8	0.96	-46.1	-55 ± 5
5	-0.10	6.5	0.98	-47.8	-54 ± 4
Average	-0.10	10.6	0.98	-46.7	-57 ± 3

In general, the individual SZP measurements appear similar and fall within the interval of the averaged SZP. Interestingly, the pattern of variability of the intercepts is quite similar to that of the SZP values, while the variation among the values of AZP at 1000 μm is much less pronounced, as described above.

In order to determine if the variability among the linear regression analysis of the five runs was statistically significant, the Comparison of Regression Lines function within the Statgraphics Centurion 19 software was used. Results of the analysis produce a p-value to compare both the intercepts and slopes between the two data sets. The results of this analysis are presented as two matrices in Figure 6, in which Panel A presents p-values comparing the intercepts of two regression lines while Panel B presents the p-values of the slope comparisons. The labels R1, R2, and so on represent the run number, which were done sequentially in time from run 1 to run 5, with run 5 being the last of the five runs.

A

	R1	R2	R3	R4	R5
R1		0.18	0.02	0.01	0.00
R2	0.18		0.23	0.06	0.02
R3	0.02	0.23		0.13	0.04
R4	0.01	0.06	0.13		0.91
R5	0.00	0.02	0.04	0.91	

B

	R1	R2	R3	R4	R5
R1		0.62	0.62	0.68	0.94
R2	0.62		0.31	0.45	0.59
R3	0.62	0.31		0.89	0.72
R4	0.68	0.45	0.89		0.73
R5	0.94	0.59	0.72	0.73	

Figure 6. In Panel A, the p-values comparing the intercepts of two linear regression lines for SZP measurement runs of a bare Nylon substrate. In Panel B, the p-values comparing the slopes of the same regression analyses are shown. Cells are color coded with green indicating no significant difference, red indicating significant difference and yellow indicating moderate significance with p-values near 0.05.

For example, in Panel A, the matrix indicates that the p-value when comparing the intercept of Run 1 (R1) with that of Run 3 (R3) is 0.02, indicating that the two intercepts are significantly different. With respect to the 95% confidence interval, green in the matrices represents two data that are not significantly different, yellow represents moderate significance with p-values at or near 0.05, and red represents significance. In Figure 6B, it is clear that there are no significant differences among any of the slopes of the regression lines of the five runs, which also seems visually apparent when examining **Error! Reference source not found.**A. However, the

analysis presented in Figure 6A indicates that there are significant differences among the intercepts of the five runs in a clear pattern. For example, Run 1 appears to have a similar intercept to Run 2, the measurement completed immediately after Run 1, but has significantly different intercepts than the others. Likewise, Run 3 has similar intercepts to the run completed immediately before (Run 2) and the run completed most immediately after (Run 4) while having significantly different intercepts than Run 1 or Run 5.

As described previously, this data suggests a significant 'drift' in sequential measurements of the same substrate. The total time for each Run is approximately 50 – 55 minutes. At each measurement position, 5 replicate measurements are taken over a matter of approximately 8 minutes. Following manual adjustment of the position and initialization of the software, the default pause is one minute to equilibrate temperature. As described previously, this effect may be due to local changes in temperature. Including longer pauses between replicate measurements, measurements at successive positions, and/or agitation of the tracer suspension between runs may have influenced these results. A future systematic study of these measurement parameters would be beneficial to fully understand their influence on the reported results. Likewise, the experiment above does not address 'inter-substrate' variability of SZP as only one substrate was measured multiple times. In a future study it would be useful to compare the SZP of multiple substrates taken from the same larger sheet of Nylon as well as from multiple lots of similarly produced Nylon sheets.

3.3 UV-Vis Analysis of Silver Coated Slide Results

Although considered a coinage metal, silver is more reactive than gold, especially in the case of the surfaces of metallic nanoparticles.[22] With silver's reactivity in mind, it is necessary to determine if the Malvern Tracer particle suspension had any adverse effects on the silver

nanoparticles adsorbed to the nylon surface. UV-Visible spectroscopy was used to measure whether the silver particles underwent a change is size or aggregation state when exposed to the tracer suspension. As described in Section 1.5, silver nanoparticles interact with visible light through the plasmon resonance. It has been demonstrated in many studies that the shape and position of the plasmon band are extremely sensitive to the size of the particles as well as the environment surrounding the particles.[23,24] Due to this, changes in the plasmon maximum and width of the plasmon band before and after exposure to the tracer particle suspension would be an indication that the suspension is causing the particle surface to dissolve or oxidize. Silver nanoparticles were adsorbed to a glass slide that was treated with a pyridine-coating polymer to form a submonolayer. The UV-Vis spectra of the control slide were compared to the UV-Vis spectra of each of the experimental slides, seen in **Error! Reference source not found.**. There were no noticable variation in any other locations aside from the peak in the trial slide spectra when compaired to the control spectrum and thus only the peaks are shown.

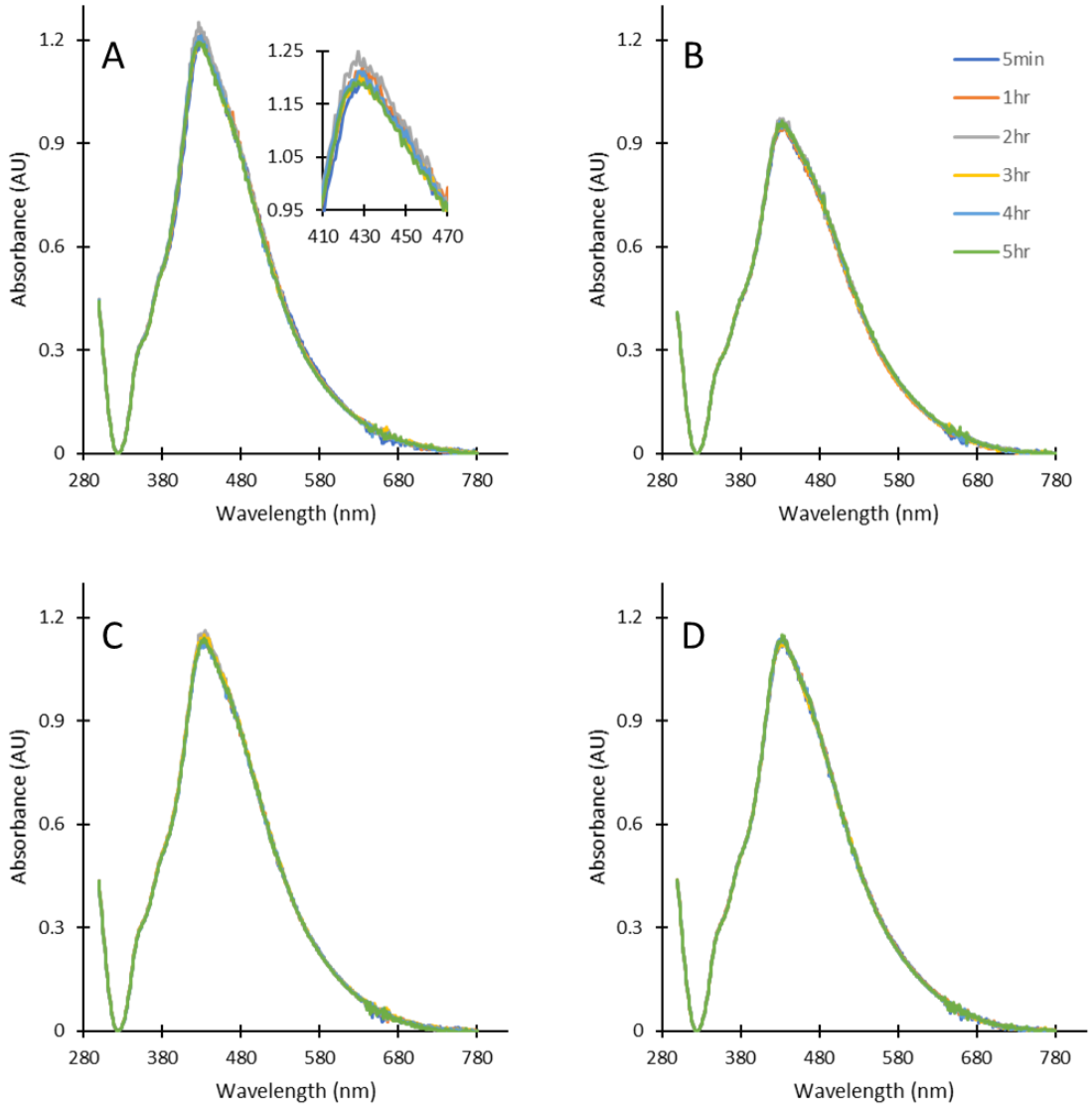

Figure 7. In Panel A, UV-visible spectra of a silver nanoparticle-coated glass slide after timed exposure to water are shown. In Panels B – D, spectra taken after multiple trials of exposing similar slides to Malvern DTS-1235 tracer particle suspensions. The labels shown in Panel B correspond to the exposure times and the colors are consistent across all panels. In Panel A, spectral variation at the plasmon maxima of the control slide is shown as an inset and is typical of the change measured among the sample slides

The λ_{max} for the samples was observed around the 430 nm wavelength. The most obvious difference from the visual analysis of the spectra, was that the max absorption of the first experimental slide was around 1 absorption units (AU) whereas the other slides all had max

absorptions around 1.2 AU, though this difference is due to typical variations in the fabrication of such slides in which the sample shown in panel B has fewer particles on the glass surface as opposed to those of Panels C and D. Since the spectra shown in each of the panels showed very little difference from the control slide or from each other, it was determined that visual analysis of the spectra was insufficient to determine if the experimental slide spectra was significantly different than the control slide spectra. Therefore, statistical analysis using single factor ANOVA testing was performed on three variables, the peak height in absorbance units, the full width at half maximum (FWHM) and the peak position in order to determine if there was a statistical difference in the spectra. The test was performed on all 24 spectra simultaneously with 6 spectra coming from the control and 6 coming from each of the three trials. The single factor ANOVA test provides a p-value for each variable tested and if the p-value is greater than 0.05 there is not a significant statistical difference between the values being tested. The p-value for the peak height was found to be 0.187, the p-value for the FWHM was found to be 0.341 and the peak height had a p-value of 0.479. Since each of the p-values from the three variables was greater than 0.05, then the experimental slides spectra are not statistically different than the control slide spectra. Since there was no statistical difference found between any of the spectra, then the sliver surface is not undergoing an apparent chemical interaction by exposure to the tracer particle suspensions.

3.4 Preliminary Surface Zeta Potential Measurements of Silver-Coated Nylon Substrates

Following confirmation that the Malvern tracer particle suspension is having no apparent effect on the silver nanoparticles, but before the more carefully designed study described in the subsequent sections of this chapter were completed, some preliminary SZP measurements were conducted. In this preliminary study, the substrates were the same Nylon sheet as used in the

remainder of the studies presented here. However, the sample holder used for silver evaporation was not optimized. The holder created a masking effect such that only a portion of the substrate was coated with silver. Likewise, the thickness of the mask created a shadowing effect such that the two substrates that were used in the preliminary study below had a heterogeneous thickness across each substrate. Likewise, the design of the holder placed the two substrates in different areas of the 'evaporation cone,' likely meaning that the two substrates also had different average silver thicknesses. Nevertheless, the surface zeta potential measurement procedure was conducted three times on each of the two silver-coated nylon substrates.

The expected results of these experiments were informed by a study conducted by Morga et al., in which surface zeta potentials were measured for silver nanoparticles immobilized on a mica substrate coated with a poly(allylamine) hydrochloride (PAH) layer using streaming potential measurements.[11] The researchers were able to model the measured SZP by using the zeta potentials of the silver nanoparticles, which they measured to be -43 mV at a pH of 9, the ZP of the mica layer, and other properties including surface coverage of silver, thickness of the PAH layer, thickness of the electrical double layer, etc. Generally speaking, the resulting SZP of the coated surface was akin to a weighted average of the ZP of the underlying substrate and surface coating, such that SZP values between the -57 mV measured for bare nylon and the -43 mV for silver nanoparticles reported by Morga et al. were expected for the preliminary studies below.[11]

The results of the three replicate runs of the first silver-coated Nylon substrate are shown in

Figure 8 Panels A – C, with Panel A depicting the results of the first replicate and Panel C showing the third replicate. Among the three panels, the slopes, intercepts and relative

position of the data are relatively consistent. The SZP values, calculated from the linear regression shown in the three panels, as well as the separate measurements of the tracer particle suspension AZP at a distance of 1000 μm from the substrate surface, are also somewhat similar, ranging from -59 mV to -67 mV. However, examination of the three replicates does indicate an increasingly positive intercept among the three trials, which in turn leads to an increasing negative SZP value.

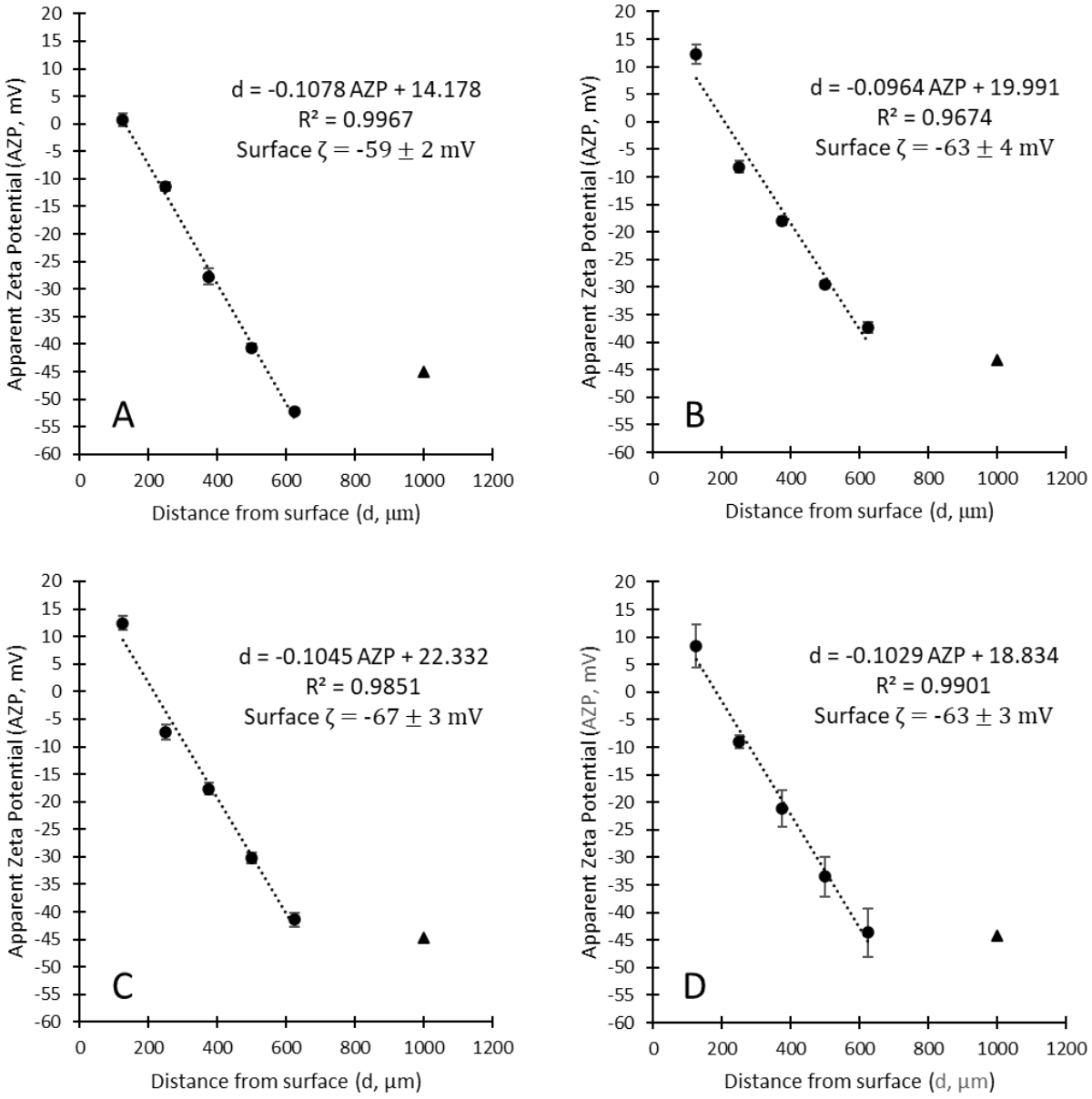

Figure 8. Surface zeta potential measurements of vacuum-evaporated silver films on a Nylon substrate. In panels A – C, the data for three measurements performed on the same film are shown, respectively. In Panel D, the average of the three replicates is shown. In each panel, ● represents the apparent zeta potential of the tracer particles at the indicated distance from the silver surface, while ▲ represents the zeta potential of the tracer particles. While the error bars in Panels A – C represent the deviation among the 5 measurements made at each distance indicated, the error bars in Panel D represent the deviation between the data in Panels A – C at the indicated distance.

When comparing these results to that shown in Table 1, the bare Nylon measurements produced similar slopes and SZP values but a different trend among the subsequent replicates. While the intercepts of the bare Nylon became less positive with successive replicates, the silver-coated substrates produced increasingly positive replicates. Likewise, successive SZP values varied in a less clear pattern with the bare Nylon as compared to the first silver coated substrate. In

Figure 8D, the averaged run data for the first substrate is shown. The average SZP of -63 ± 3 mV is slightly more negative than that calculated for bare Nylon of -57 ± 3 mV (cf. Figure 6B). When comparing the two averages, the more positive intercept of the silver-coated Nylon is apparent, as is the increased variability in the run data used to calculate the average. While the average standard deviation among the five points used in the regression analysis of Figure 6B is 1.9 mV, the average standard deviation of the data in

Figure 8D is 3.3 mV.

The data for the replicate runs of the second substrate are shown in Figure 9, with Panels A – C showing the successive runs of the substrate. Like the first substrate, the intercepts of the regression analyses became more positive during successive runs and as such, the SZP measurements of the second substrate became more negative. In the case of the second substrate the variation of SZP values was much more pronounced, ranging from -38 ± 2 mV to -61 ± 6 mV. Unlike the first substrate or the bare Nylon trials, the slope of the regression analyses of the

second substrate also seemed to vary quite a bit. In Figure 9D, the averaged data for the SZP of the second substrate is shown. The averaged SZP value of -47 ± 3 mV is somewhat different than the first substrate, which appeared to have a more negative SZP than bare Nylon. As was described above, the increased variation among the replicates of substrate 2 is also evident in Figure 9D. While the average standard deviation among the five points used in the regression analysis of Figure 6B is 1.9 mV, the average standard deviation of the data in Figure 9D is 3.6 mV. However, while the error bars in

Figure 8D were fairly uniform, the changing slopes of the replicate data in Figure 9, produced average values in Figure 9 that had decreasing variability with increasing distance from

the substrate surface.

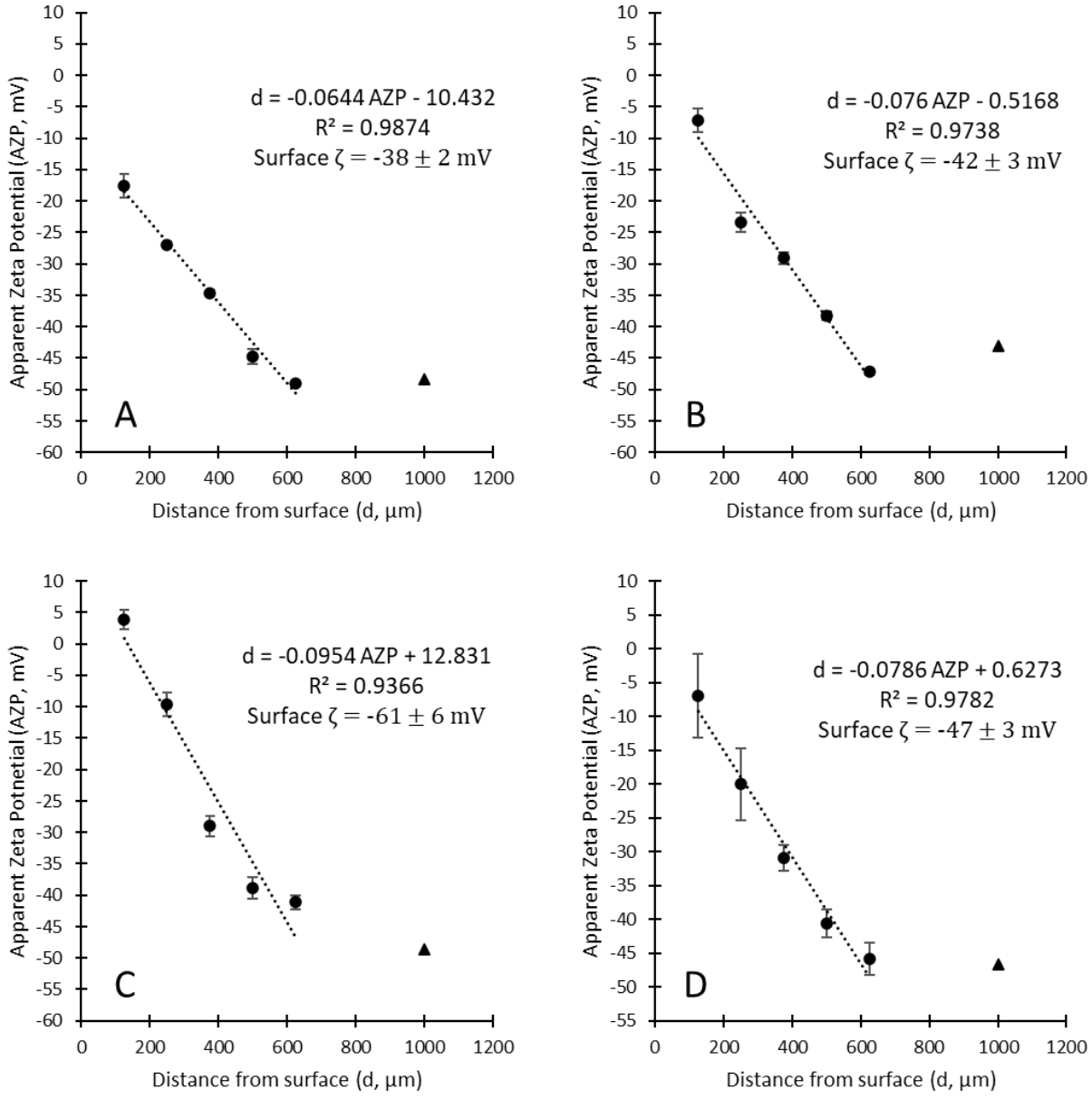

Figure 9. Surface zeta potential measurements of vacuum-evaporated silver films on a Nylon substrate. In panels A – C, the data for three measurements performed on the same film are shown, respectively. In Panel D, the average of the three replicates is shown. In each panel, ● represents the apparent zeta potential of the tracer particles at the indicated distance from the silver surface, while ▲ represents the zeta potential of the tracer particles. While the error bars in Panels A – C represent the deviation among the 5 measurements made at each distance indicated, the error bars in Panel D represent the deviation between the data in Panels A – C at the indicated distance.

To better compare the replicate runs of the silver-coated Nylon substrates with that of bare Nylon, single-factor ANOVA was performed on the SZP values calculated for the 3 replicate runs of each silver coated substrate and the five replicate runs of the bare Nylon substrate. The analysis produced a p-value of 0.056, indicating that the differences in the data sets were not statistically significant. This ANOVA analysis would seem to indicate that the SZP value of silver-coated nylon was generally the same as that of bare nylon. However, given that the p-value was quite close to 0.05, which would indicate significance, t-tests were conducted on each of the combinations of the data of the three substrates. To begin, an F-test was performed on each combination to determine if the variance among the replicate data were equal. These tests indicated equal variance between the 2 silver coated substrates ($F > 0.05$ [0.09]) and between bare Nylon and the first of the two silver coated substrates ($F>0.05$ [0.2]). However, the F-test indicated an unequal variance between the data SZP replicates of bare nylon and the second silver-coated substrate ($F<0.05$ [0.008]). As such, the proper t-test was conducted using the variance information obtained in the F-test. Interestingly, the t-tests indicated that the replicate data from the first silver-coated substrate (Figure 8) was significantly different from bare Nylon (two-tailed p-value of 0.049) while the other comparisons were not significantly different. The two-tailed p-value for the t-test comparing the two silver-coated substrates was 0.1 while the two-tailed p-value comparing bare Nylon with the second silver-coated substrate was 0.3.

To compare the regression data among the replicate runs of the same silver-coated substrates, as well as compare the averaged data of the silver-coated substrates with bare Nylon,

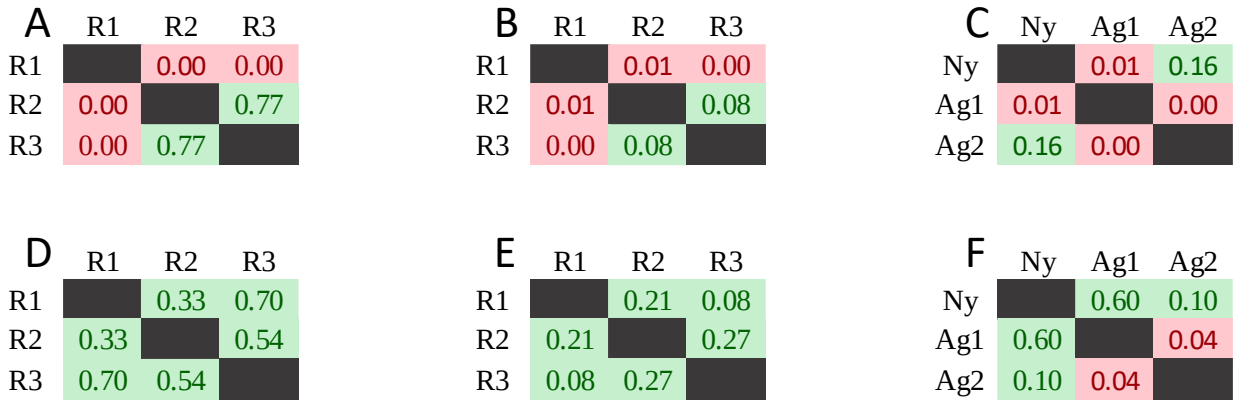

Figure 10. Panels A and B compare the intercepts of the replicate runs of the first and second silver-coated substrates, respectively, while Panels D and E compare the slopes of the same regression analyses. In Panels C and F, the intercepts and slopes, respectively, are compared among the two silver-coated substrates (cf. Figure 8D for Ag1 and Figure 9D for Ag2) and the bare Nylon replicates (cf. Figure 5B). Cells are color coded with green indicating no significant difference, red indicating significant difference and yellow indicating moderate significance with p-values near 0.05.

similar analyses were conducted with the Statgraphics Centurion 19 software package as was described in section 3.2. Figure 10, Panels A and D compare the replicate run regression analyses for the intercepts and slopes, respectively, for the first silver-coated nylon substrate while Panels B and E compare similar data for the second silver-coated substrate. Similar to the data presented in Figure 6B, the slopes of the regression analyses from the two substrates (Figure 10, Panels D and E), do not vary significantly among their successive runs. Also similar to bare Nylon (cf. Figure 6A), the intercepts of the two silver coated substrates (Figure 10, Panels A and B) do vary significantly. However, the pattern appears to be different. For bare Nylon, each successive replicate was insignificantly different from its nearest neighbor, such as when comparing R1 to R2, but was generally significantly different from other replicates. In the case

of the two silver coated substrates, replicate run #1 (R1) is significantly different from both the second (R2) and third (R3) replicate runs, while the intercepts are not significantly different between the second and third replicates. This change in pattern between bare Nylon and the silver-coated Nylon may indicate differing behavior of the substrates under the conditions of the SZP measurement. When comparing the intercepts (Figure 10C) and slopes (Figure 10F) between the averaged bare Nylon replicate data (cf. Figure 5B) and the averaged replicate data of the two silver-coated substrates (cf.
Figure 8D and Figure 9D), significant differences can be seen between the intercept of silver-coated substrate #1 (Ag1) and both of the other two samples, while when comparing the slopes of the averages, silver-coated substrates #1 and #2 appeared to be significantly different while the differences when comparing the Nylon slope to either of the silver-coated substrates were not significant.

In general, the data collected in this preliminary study led to more questions than answers. The most noticeable trends in the data were that successive runs on the same substrate produced increasingly negative results that seemed to vary in a pattern different from bare Nylon. Likewise, the two silver-coated substrates had remarkably different SZP data that produced averaged regression analyses that were significantly different from each other. The large difference between the SZP values could be explained by sample one having less silver than sample two or it could be due to there being little difference between the SZP of nylon and thermally evaporated silver in general. If the ZP of thermally-evaporated silver is similar to that reported by Morga et al., an explanation for the increasingly negative SZP measurements could be that the amount and/or exposed surface area of silver on the Nylon substrate was changing during the successive measurements.[11] In order to better investigate these results, a more

thorough study with a larger number of samples and better control over the amount of silver on each substrate was conducted and is described in the following section.

3.5 Silver Coated Substrate Runs Trial Results

Following completion of the preliminary studies described above, a more careful study of SZP measurements of silver-coated Nylon was conducted. To begin, a new sample holder was constructed for the thermal evaporator that allowed for the pre-cut Nylon substrates to be held in place without a shadowing effect and such that the entire Nylon face could be coated, i.e., the silver coating thickness across a substrate used in this portion of the study should be more uniform. Likewise, the holder was designed such that the Nylon substrates were spaced equidistant from the center axis of the silver pellet used for evaporation to better ensure that the silver coatings among all, the substrates used in this section of the study were more consistent. For this portion of the study, 9 substrates were taken from a set of 15 Nylon substrates that all received silver coatings during the same evaporation run. See sections 2.2.1 and 2.2.5 for a description of the processes used to prepare the substrates.

This study was designed to examine both the inter-substrate variability of SZP measurements as well as the intra-substrate variability of SZP measurements resulting from successive measurements on the same substrate. For the nine substrates used, three were subjected to the SZP measurement protocol once. In the subsequent discussion in this section, these three substrates are labeled A, B and C. Similarly, three of the 9 substrates were each subjected to the SZP measurement protocol twice and are labeled E, F, and G in the following discussion. In each case, the second SZP measurement protocol was conducted immediately following the completion of the first. In a similar fashion, the SZP measurement protocol was

conducted three successive times on each of three silver-coated Nylon substrates. In the following discussion, these substrates are labeled I, J, and K.

The results of the SZP measurements are shown in the following three Figures. Among the three Figures, the following colors and symbols are consistently used, as needed, to represent apparent zeta potentials of the first (●), second (■), and third (◆) successive runs on each substrate. Likewise, the following colors and symbols are used to represent the apparent zeta potential of the tracer particles, measured at 1000 μm from the substrate surface during the first (▲), second (◆), and third (●) successive runs on each substrate. In each Figure, the data for each of the three separate substrates are paneled and labeled as described above, while the lower right panel in each Figure presents the average of the data presented in the other three panels. While the error bars in the first three panels of each Figure represent the deviation among the 5 measurements made at each distance indicated, the error bars in the bottom right panel represent the deviation between the data of the other three panels at the indicated distance. Within each panel of the three Figures, the dotted lines refer to the linear regression best-fit line of the data of corresponding color. In Figure 11, the equations of the lines of best-fit are also shown within each panel. The intercept of these equations, along with the ZP of the tracer particles as measured at 1000 μm from the substrate surface are used to calculate SZP (cf. Equation 6). The Figures indicate the calculated value of SZP as "Surface ζ." In Figure 12 and Figure 13, only the SZP values are shown. The linear regressions data and resulting SZP values for each substrate

and run are also summarized in Table 2.

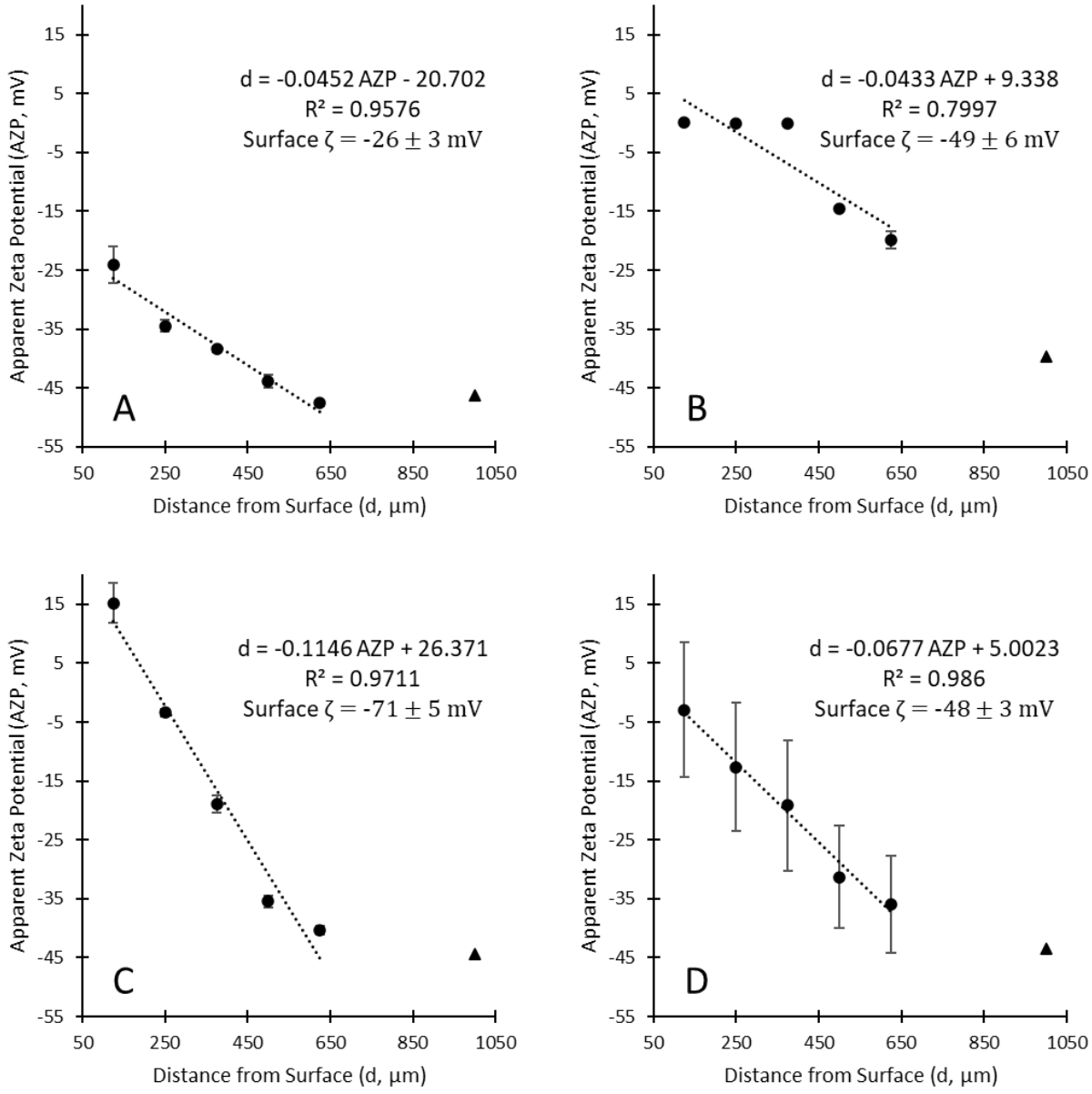

Figure 11. Surface zeta potential measurements of vacuum-evaporated silver films on Nylon substrates. In panels A – C, the data for three separate films are shown, respectively. In Panel D, the average of the three replicates is shown. In each panel, ● represents the apparent zeta potential of the tracer particles at the indicated distance from the silver surface, while ▲ represents the zeta potential of the tracer particles. While the error bars in Panels A – C represent the deviation among the 5 measurements made at each distance indicated, the error bars in Panel D represent the deviation between the data in Panels A – C at the indicated distance.

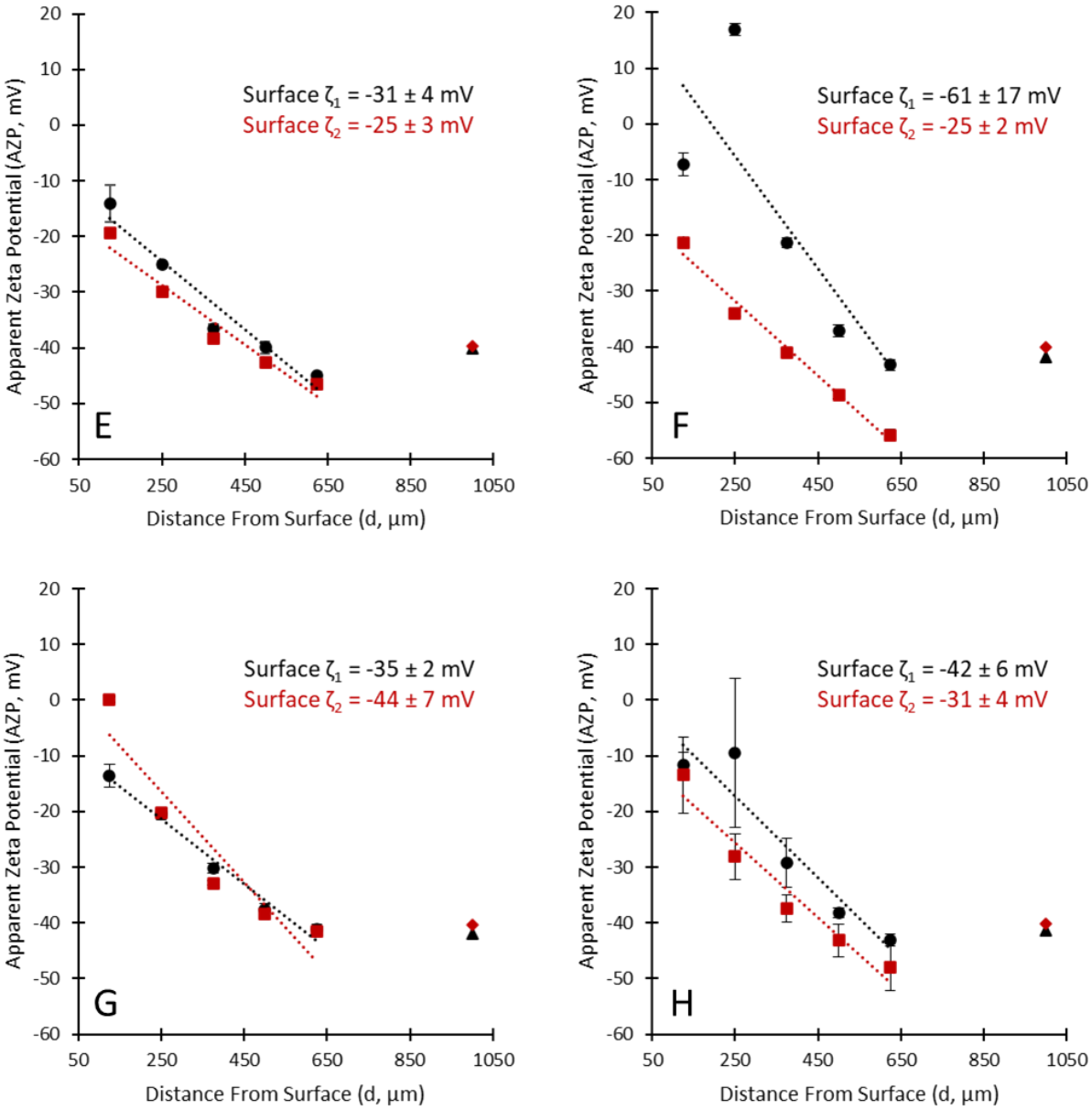

Figure 12. Two, sequential Surface zeta potential measurements of vacuum-evaporated silver films on a Nylon substrate. In panels E – G, the data for the two sequential measurements of three separate films are shown, respectively. In Panel H, the average of the three replicates is shown. In each panel, ● (run 1) and ■ (run 2) represent the apparent zeta potential of the tracer particles at the indicated distance from the silver surface, while ▲ (run 1) and ◆ (run 2) represent the zeta potential of the tracer particles. While the error bars in Panels E – G represent the deviation among the 5 measurements made at each distance indicated, the error bars in Panel

H represent the deviation between the data in Panels E – G at the indicated distance.

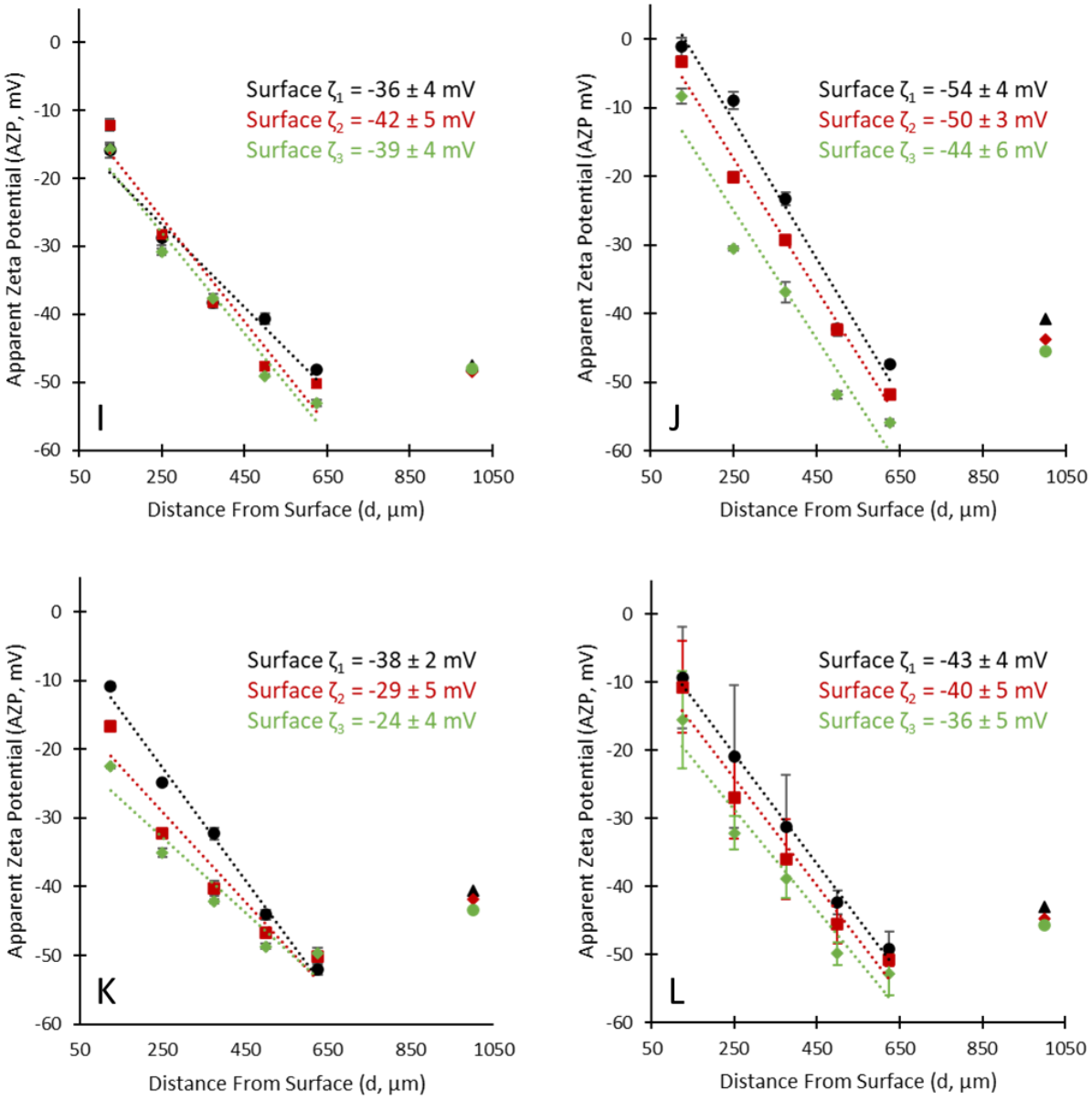

Figure 13. Three, sequential Surface zeta potential measurements of vacuum-evaporated silver films on a Nylon substrate. In panels I – K, the data for the three sequential measurements of three separate films are shown, respectively. In Panel L, the average of the three replicates is shown. In each panel, ● (run 1), ■ (run 2), and ◆ (run 3) represent the apparent zeta potential of the tracer particles at the indicated distance from the silver surface, while ▲ (run 1), ◆ (run 2), and ● (run 3) represent the zeta potential of the tracer particles. While the error bars in Panels I – K represent the deviation among the 5 measurements made at each distance indicated, the error bars in Panel L represent the deviation between the data in Panels I – K at the indicated distance.

Table 2. Summary of Linear Regression Analysis and calculated surface zeta potential for each measurement of a silver-coated Nylon substrate exposed to a varying number of runs, as well as the averaged data. Graphical representations of this data are shown in Figure 11-Figure 13.

		Linear Regression Analysis			**AZP at**	**Surface Zeta**
Sample / Figure Panel	**Run**	*Slope (mV/µm)*	*Intercept (mV)*	*Coefficient of Determ. (R^2)*	**1000 µm (mV)**	**Potential (mV)**
A	1	-0.05	-20.7	0.96	-46.3	-26 ± 3
B	1	-0.04	9.3	0.80	-39.6	-49 ± 6
C	1	-0.11	26.4	0.97	-44.4	-71 ± 5
D	*Average*	*-.007*	*5.0*	*0.99*	*-43.4*	*-48 ± 3*
E	1	-0.06	-9.1	0.95	-40.0	-31 ± 4
	2	-0.05	-15.2	0.95	-39.7	-25 ± 3
	Average	*-0.06*	*-12.2*	*0.95*	*-39.9*	*-28 ± 3*
F	1	-0.10	19.5	0.68	-41.9	-61 ± 17
	2	-0.07	-15.0	0.98	-40.1	-25 ± 2
	Average	*-0.08*	*2.2*	*0.88*	*-41.0*	*-43 ± 8*
G	1	-0.06	-6.8	0.98	-41.9	-35 ± 2
	2	-0.08	3.9	0.89	-40.4	-44 ± 7
	Average	*-0.07*	*-1.5*	*0.94*	*-41.2*	*-40 ± 4*
H	*1*	*-0.07*	*1.2*	*0.90*	*-41.3*	*-42 ± 6*
	2	*-0.07*	*-8.8*	*0.95*	*-40.1*	*-31 ± 4*
	Average	*-0.07*	*-3.8*	*0.97*	*-40.7*	*-37 ± 3*
I	1	-0.06	-11.5	0.94	-47.5	-36 ± 4
	2	-0.08	-6.6	0.94	-48.4	-42 ± 5
	3	-0.07	-9.4	0.97	-48.0	-39 ± 3
	Average	*-0.07*	*-9.2*	*0.96*	*-48.0*	*-39 ± 4*
J	1	-0.10	13.1	0.97	-40.7	-54 ± 4
	2	-0.10	6.3	0.99	-43.8	-51 ± 3
	3	-0.09	-1.7	0.94	-45.6	-44 ± 6
	Average	*-0.10*	*5.9*	*0.98*	*-43.3*	*-49 ± 3*
K	1	-0.08	-2.4	0.99	-40.6	-38 ± 2
	2	-0.07	-12.8	0.93	-41.8	-29 ± 5
	3	-0.05	-19.2	0.92	-43.4	-24 ± 4
	Average	*-0.07*	*-11.4*	*0.96*	*-42.0*	*-31 ± 3*
L	*1*	*-0.08*	*-0.3*	*0.99*	*-43.0*	*-43 ± 4*
	2	*-0.08*	*-4.4*	*0.96*	*-44.7*	*-40 ± 5*
	3	*-0.07*	*-10.1*	*0.95*	*-45.6*	*-36 ± 5*
	Average	*-0.08*	*-4.9*	*0.97*	*-44.4*	*-40 ± 4*

The data presented in Table 2 corresponds to the data presented in Figure 11– Figure 13. The rows labeled A – C (cf. Figure 11) indicate the regression analysis information and calculated SZP for three substrates in which the SZP measurement was completed once. The row labeled D, which corresponds to Figure 11D, indicates the average data for substrates A – C in which the individual measurements at each measurement position for the three substrates were

first averaged together, followed by linear regression analysis and calculation of the SZP. Similarly, rows E, F, and G correspond to substrates in which the SZP measurement protocol was completed twice (cf. Figure 12E – Figure 12G). 'Run 1' indicates the result of the first SZP measurement while 'Run 2' indicates the second SZP measurement on the same substrate. 'Average' indicates regression data that was found by averaging the measurement position data for the two runs. In Row H (cf. Figure 12H) of Table 2, the averaged data of the first runs of the three substrates (Run 1 of E, F, and G) and the second runs are shown. The Average regression analysis data shown in Row H was found by first averaging together the measurement-position-specific data for the 6 total runs of substrates E, F, and G. In a similar fashion to rows E, F, and G, Rows I, J, and K (cf. Figure 13I - K) represent the data analysis completed for the three substrates that were each measured three times. The averaged data of Row L (cf. Figure 13L) in Table 2 is organized similarly to that described for Row H.

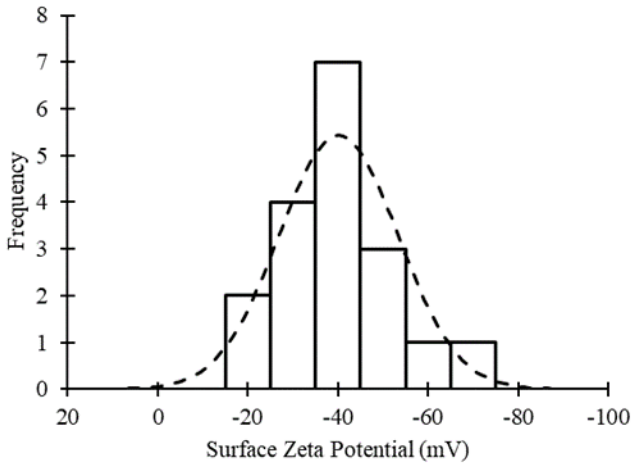

Figure 14. Histogram of the data presented in Table 2 of the 18 SZP measurement procedures completed on the nine silver-coated Nylon substrates. The dashed line in the figure represents a hypothetical normal distribution with the same mean, standard deviation, and area as the actual data.

Among the 18 individual SZP measurement procedures completed on the 9 substrates, there is considerable variation, with the SZP value ranging from -26mV to -71 mV. Interestingly, these values are outside of the bounds of bare Nylon (-57±3 mV, cf. Section 3.2) and the value of ZP reported for silver of ca. -43 mV by Morga et al. However, as can be seen in the histogram in Figure 14, the data are centered around -40 mV and when compared to a hypothetical normal distribution (dashed line) with the same mean, standard deviation and area, the data collected from the 18 SZP measurements of the 9 substrates appear to be normally distributed. The average value for SZP of silver thermally evaporated onto a Nylon substrate at pH 9.2 and a temperature of 25 °C is -40±13 mV. To further confirm the normal distribution of the data, single factor ANOVA was completed by separating the data into three subsets. Subset 1 contained the SZP values for substrates A, B, and C (the substrates measured once, while subset 2 contained the averaged SZP values for the substrates measured twice (E, F, and G) and subset 3 contained the SZP values for the substrates measured thrice (I, J, and K). The p-value for this ANOVA test was 0.63, indicating that the subsets were not significantly different.

To better compare the replicate runs of the silver-coated Nylon substrates with that of bare Nylon, single-factor ANOVA was performed on the SZP values calculated for the two or three replicate runs of silver-coated substrates E, F, G, I, J, and K and the five replicate runs of the bare Nylon substrate. This analysis produced a p-value of 0.007, indicating a significant difference among the data groups. When performing ANOVA of the silver-coated Nylon SZP values without including the bare Nylon data, the p-value was 0.24. Unlike the similar analysis that was described in the preliminary study (cf. Section 3.4), the combination of these two ANOVA experiments conclusively indicate that the silver-coated Nylon substrates have a significantly different SZP as compared to bare Nylon.

In Section 3.4, the preliminary study indicated a pattern of increasingly negative SZP values after successive runs on the same silver-coated substrate. A potential explanation of this phenomenon may be that silver is being removed from the surface during successive measurements. While the two substrates in Section 3.4, both exhibited an increasingly negative SZP, the substrates in this study did not. In fact, when comparing the values reported in Table 2 for the 6 substrates that were subjected to the SZP measurement procedure multiple times, the SZP of the last run is more positive than the first run 67% of the time, similar to the observation among the replicate runs of the bare Nylon. Similar to that case, the change in SZP may be indicating a change in surface chemistry or may simply be an artifact of the measurement related to temperature equilibration. Given that the substrate holder was refashioned to better allow for complete and homogeneous coatings than in the preliminary study, the lack of a clear trend of increasingly negative SZP measurements does not preclude the removal of silver from the surface during the measurements. Rather, the presence of more silver on each substrate may limit the likelihood that bare Nylon is being exposed during the measurements.

To better compare the differences between replicate SZP measurements on the same substrate, ANOVA was completed by arranging the data from the nine substrates into three subsets. Subset 1 contained the 9 SZP values from the first run completed on a substrate (Run 1 on substrates A, B, C, E, F, G, I, J, and K). Subset 2 contained the 6 SZP values from the second run on a substrate (Run 2 on substrates E, F, G, I, J, and K) and subset 3 contained the Run 3 SZP values from substrates I, J, and K. The p-value for this analysis was 0.39, indicating that the SZP values from subsequent replicates are not significantly different.

While the SZP values among the substrates do not seem to be significantly different from each other, statistical analysis of the regression data, using the Comparison of Regression Lines

function within the Statgraphics Centurion 19 software was nevertheless completed to determine if any patterns emerged. For example, in Section 3.2 (cf. Figure 6) among the 5 replicates of the bare Nylon measurement, the slope and intercept varied in a predictable pattern. This same analysis was performed among the 6 silver-coated Nylon substrates and the results are summarized in Table 3 below. In the Table, the p-values resulting from comparing the slopes and intercepts of the regression analyses of two replicate measurements are shown. The letter of each replicate corresponds to the substrate label of the 9 substrates (E, F, G, I, J, and K) while N refers to the bare Nylon substrate described in Section 3.2. The number next to the letter describes the run number. For example, G2 signifies the second run of substrate G.

Table 3. Summary of the statistical analysis of comparing regression analyses of replicate SZP measurements made on the silver coated Nylon substrates described above in this section (E, F, G, I, J, and K) as well as the bare Nylon substrate described in Section 3.2 (noted as N in this table. Cells are color coded with green indicating no significant difference, red indicating significant difference and yellow indicating moderate significance with p-values near 0.05.

		p-values resulting from comparison of regression analysis data	
Replicate #1	**Replicate #2**	*Intercept*	*Slope*
E1	E2	0.71	0.02
F1	F2	0.02	0.44
G1	G2	0.54	0.22
I1	I2	0.71	0.31
J1	J2	0.05	0.67
K1	K2	0.08	0.21
N1	N2	0.18	0.62
I1	I3	0.21	0.30
J1	J3	0.01	0.68
K1	K3	0.01	0.04
N1	N3	0.02	0.62
I2	I3	0.45	0.88
J2	J3	0.03	0.89
K2	K3	0.37	0.48
N2	N3	0.23	0.31

Similar to the results presented in Figure 6 of Section 3.2, the replicate measurements of each silver-coated Nylon substrate appear to be similar to the next successive replicate measurement while being less similar to more removed replicates. When comparing Run 1 and Run 2 for the

six silver-coated substrates in the table, both the slopes and the intercepts of the regression analysis are significantly different 17% of the time, with respect to the 95% confidence interval. However, when comparing Run 1 and Run 3 among the three silver-coated Nylon substrates, the intercepts are significantly different 67% of the time. This difference only occurs 33% of the time when comparing Run 2 and Run 3 of the same replicates. This pattern is similar to that seen in Figure 6 of Section 3.2 and may indicate a measurement drift as described in Section 3.2 related to temperature equilibration or may indicate a gradual change in the substrate surface during the measurement.

To further explore the possibility of a change in the substrate surface, similar statistical analysis was performed on the regression data of the 9 substrates in which the data was put in three subsets. Subset 1 contained the SZP regression data of the first (or only) replicate measurement of each of the nine substrates. Likewise, Subset 2 contained the SZP regression data of the second replicate runs of substrates E, F, G, I, J, and K and Subset 3 contained the SZP regression data from the third replicate runs of Substrates I, J, and K. The results of this analysis are presented as a series of matrices in Figure 15, in which Panels A, C, and E present p-values comparing the intercepts of subset data indicated and Panels B, D, and F present the p-values of the slope comparisons. As in previous, similar Figures, the letter is the substrate identifier while the number identifies the Run number. For example, in Panel C, the matrix indicates that the p-value when comparing the intercepts of the second run of substrate E (E2) with the second run of substrate I (I2) is 1.00, indicating that the two intercepts are not significantly different. With respect to the 95% confidence interval, green in the matrices represents two data that are not significantly different, yellow represents moderate significance with p-values at or near 0.05, and red represents significance. When comparing the matrices, it is evident that the replicate

measurements become more similar as more replicate measurements are completed. Among the first replicate runs, the regression intercepts of replicate runs are significantly different from each other 64% of the time, while for the second and third replicate data, the intercepts are significantly different 60% and 0% of the time, respectively. Likewise, among the first replicate runs, the regression slopes of replicate runs are significantly different from each other 39% of the time, while for the second and third replicate data, the slopes are significantly different 20% and 0% of the time, respectively. While there is potential that this trend is related to the reduced sample size of '3rd replicate' data as compared to the '1st replicate' data, there also potential that this trend is also indicative of the measurement itself affecting the surface, though with diminishing effect among successive replicates. This trend may indicate that the measurement may cause a change to the silver on the substrate surface, perhaps in terms of amount, surface roughness, etc., that diminishes the heterogeneity of the surfaces that is typical of vacuum evaporation.

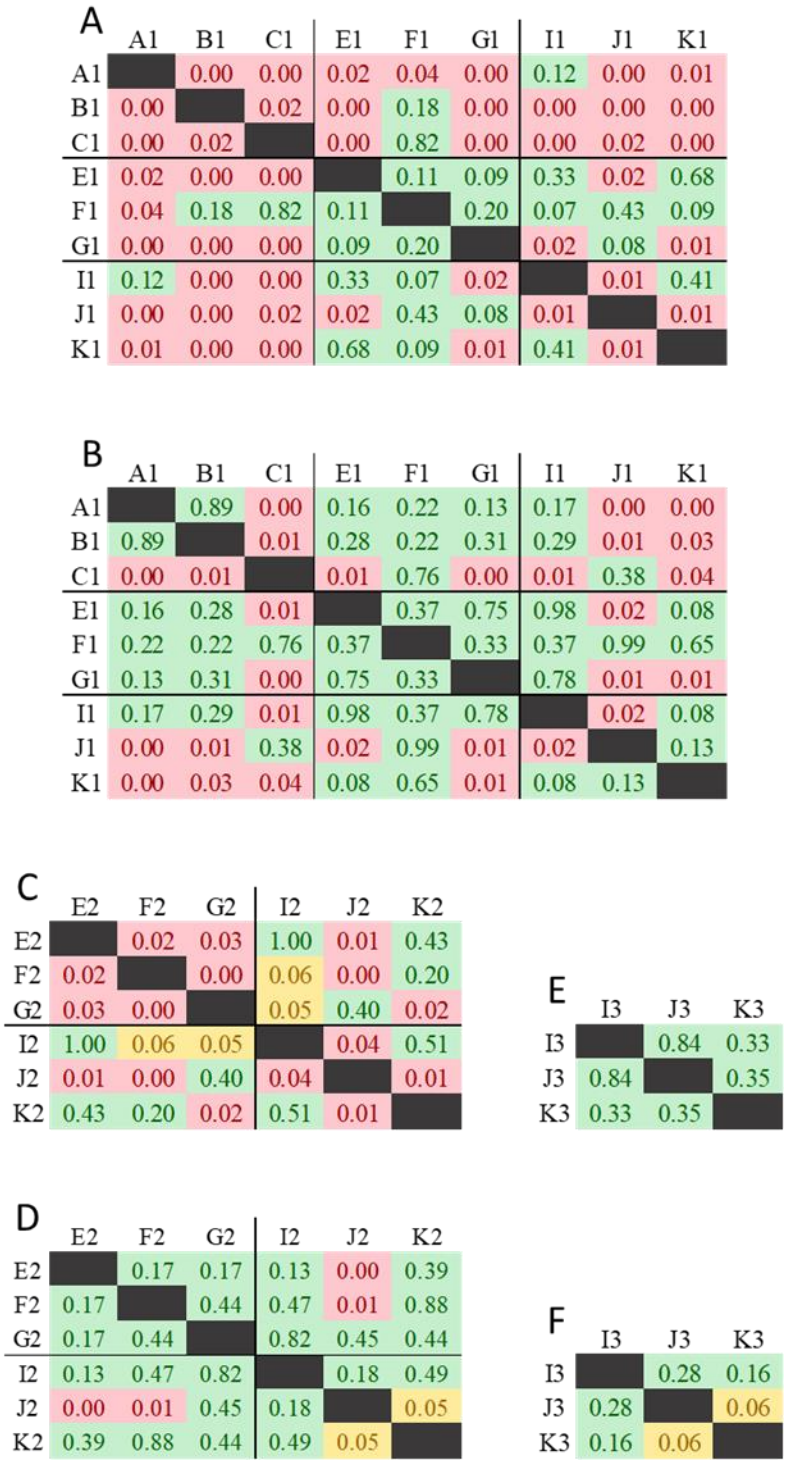

Figure 15. In Panel A, the p-values comparing the intercepts of two linear regression lines for SZP measurement runs of a silver-coated Nylon substrate are shown. In Panel B, the p-values comparing the slopes of the same regression analyses are shown. The p-values comparing the

intercepts and the slopes of two linear regressions lines for SZP measurement runs of the second run of a silver-coated Nylon substrate are shown is Panel C and D, respectively. The p-values comparing the intercepts and the slopes of two linear regressions lines for SZP measurement runs of the third run of a silver-coated Nylon substrate are shown is Panel E and F, respectively. Cells are color coded with green indicating no significant difference, red indicating significant difference and yellow indicating moderate significance with p-values near 0.05.

3.6 pH Trial Results

The projects next goal was to obtain SZP data for the silver coated substrates at different pH values. The averaged pH data for the for pH 7.10 and 9.95 can be seen in Figure 16 and Figure 17 respectively.

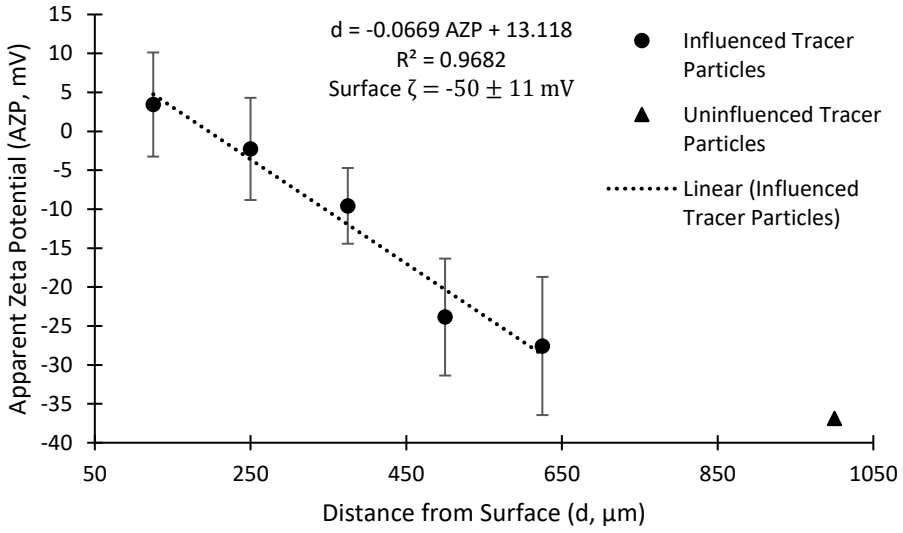

Figure 16. Averaged surface zeta potential measurements of vacuum-evaporated silver films on a Nylon substrate using Malvern zeta potential transfer standard diluted to pH 7.10.

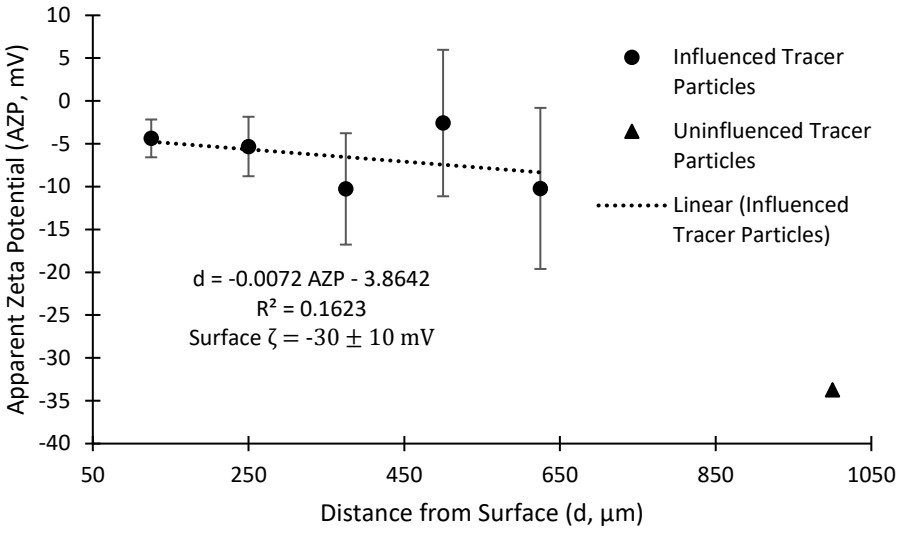

Figure 17. Averaged surface zeta potential measurements of vacuum-evaporated silver films on a Nylon substrate using Malvern zeta potential transfer standard diluted to pH 9.95.

The data for the pH trials have the highest error in the calculated SZP at ± 11 mV for pH 7.10 and ± 10 mV for pH 9.95. The dilution of the zeta potential transfer standard with pH buffer (cf. section 2.5.7) proved to be the wrong approach to obtain tracer suspensions at the desired pH. This was obvious by the pH data for pH 9.95 having an R-squared value of 0.1623 despite being the closest to the original tracer suspension pH of 9.2. This trial resulted in the project moving away from the zeta potential transfer standard provided by Malvern and creating new suspensions to measure SZP at varying pH values.

3.7 Silica pH Trial Results

The devised solution was to use silica nanoparticles suspended in buffer solution of the desired pH (cf. section 2.2.4). The SZP data for each substrate is displayed in Figure 18, Figure 20Figure 22. Among these Figures, the following colors and symbols are consistently used, as needed, to represent apparent zeta potentials of the first (●), second (■), and third (◆) successive

runs on each substrate. Likewise, the following colors and symbols are used to represent the apparent zeta potential of the tracer particles, measured at 1000 μm from the substrate surface during the first (▲), second (◆), and third (●) successive runs on each substrate. In each Figure, the data for each of the three separate substrates are paneled and labeled as described above, while the lower right panel in each Figure presents the average of the data presented in the other three panels. While the error bars in the first three panels of each Figure represent the deviation among the 5 measurements made at each distance indicated, the error bars in the bottom right panel represent the deviation between the data of the other three panels at the indicated distance. Within each panel of the three Figures, the dotted lines refer to the linear regression best-fit line of the data of corresponding color. The Figures indicate the calculated value of SZP as "Surface ζ." This data is also presented in Table 4 with the linear regression data included. The average SZP data for each pH, shown in Figure 19, Figure 21 and Figure 23, display the equation of the best-fit line and the R^2 values in addition to the calculated SZP. All SZP were calculated using the intercept from the equation of the best-fit line and the tracer particle ZP at 1000 μm from the sample surface (cf. Equation 6).

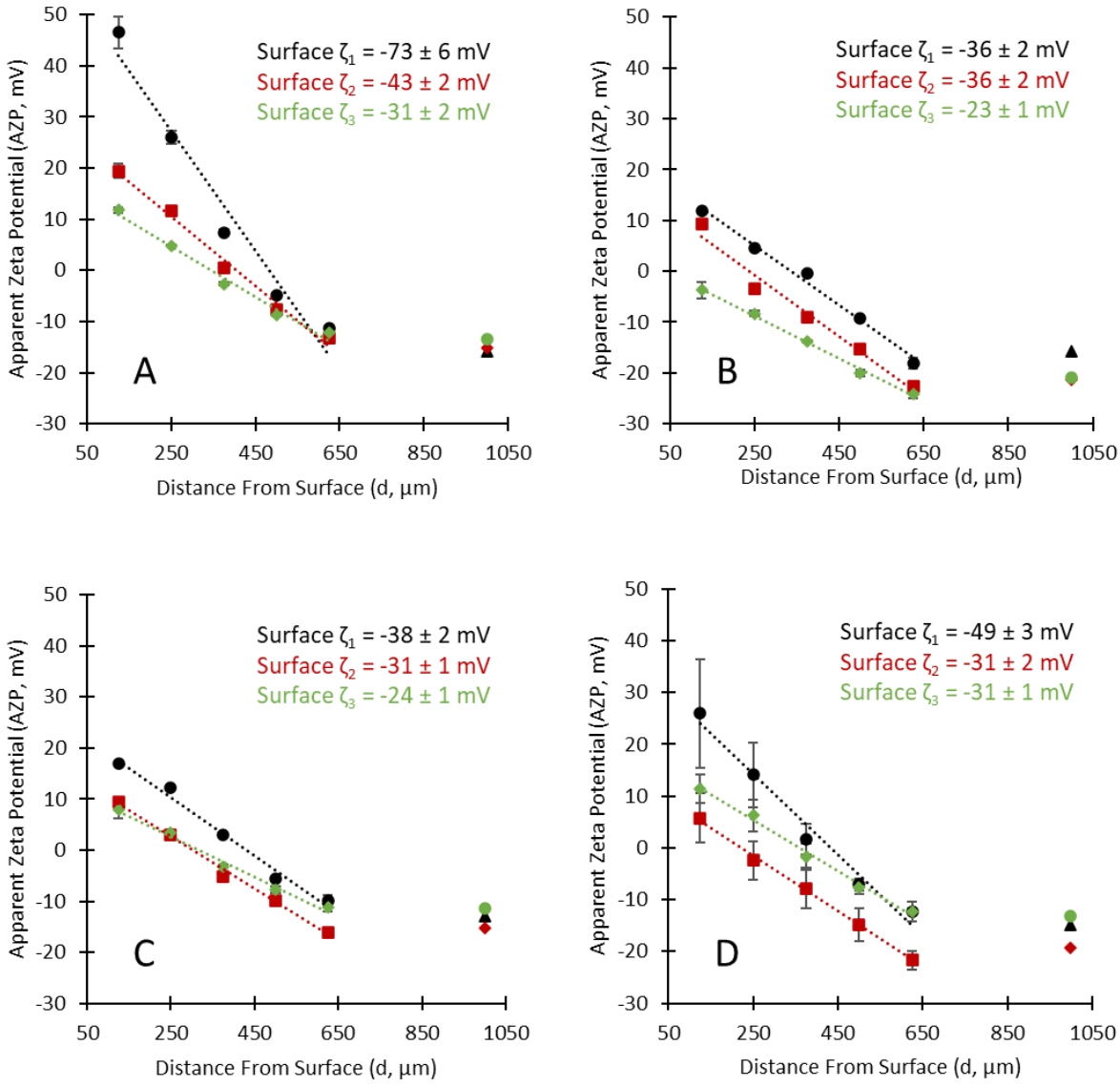

Figure 18. Surface zeta potential measurements of vacuum-evaporated silver films on a Nylon substrate using pH 5 silica tracer suspension. In panels A – C, the data for the three separate films are shown, respectively. In Panel D, the average of each sample is shown with, ●, ■, and ◆ representing trial 1, 2 and 3 respectively instead of run 1, 2 and 3 as found in Panel A – C. In each panel, ● (run 1), ■ (run 2), and ◆ (run 3) represent the apparent zeta potential of the tracer particles at the indicated distance from the silver surface, while ▲ (run 1), ◆ (run 2), and ● (run 3) represent the zeta potential of the tracer particles. While the error bars in Panels A – C represent the deviation among the 5 measurements made at each distance indicated, the error

bars in Panel D represent the deviation between the data in Panels A – C at the indicated distance.

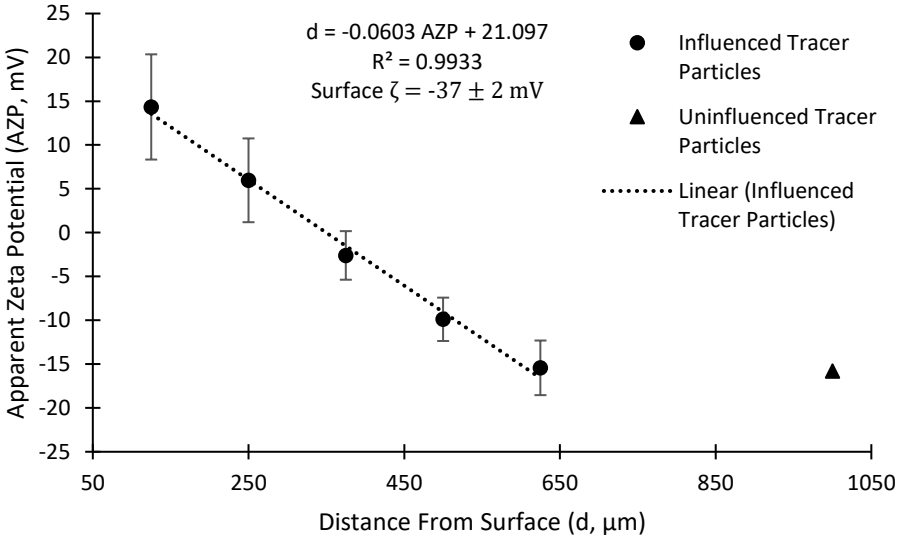

Figure 19. Averaged surface zeta potential measurements of vacuum-evaporated silver films on a Nylon substrate using pH 5 silica nanoparticle tracer suspension.

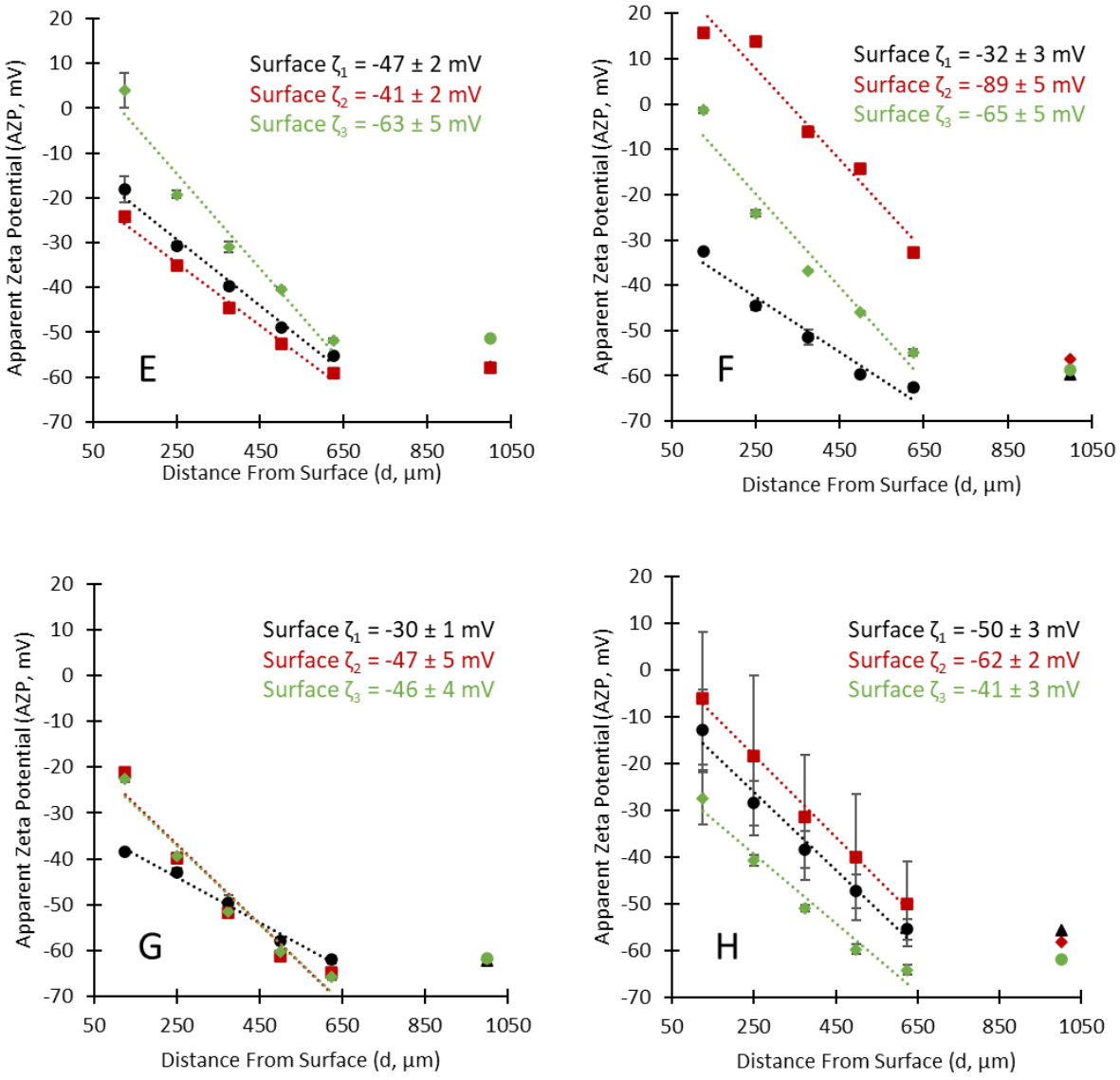

Figure 20. Surface zeta potential measurements of vacuum-evaporated silver films on a Nylon substrate using pH 7 silica tracer suspension. In panels E – G, the data for the three separate films are shown, respectively. In Panel H, the average of each sample is shown with, ●, ■, and ◆ representing trial 1, 2 and 3 respectively instead of run 1, 2 and 3 as found in Panel E – G. In each panel, ● (run 1), ■ (run 2), and ◆ (run 3) represent the apparent zeta potential of the tracer particles at the indicated distance from the silver surface, while ▲ (run 1), ◆ (run 2), and ● (run 3) represent the zeta potential of the tracer particles. While the error bars in Panels E – G represent the deviation among the 5 measurements made at each distance indicated, the error

bars in Panel H represent the deviation between the data in Panels E – G at the indicated distance.

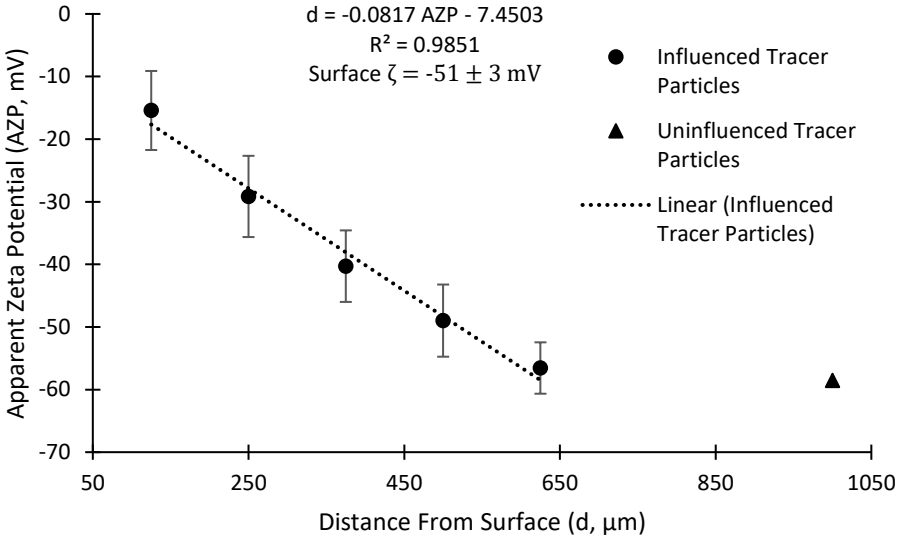

Figure 21. Averaged surface zeta potential measurements of vacuum-evaporated silver films on a Nylon substrate using pH 7 silica nanoparticle tracer suspension.

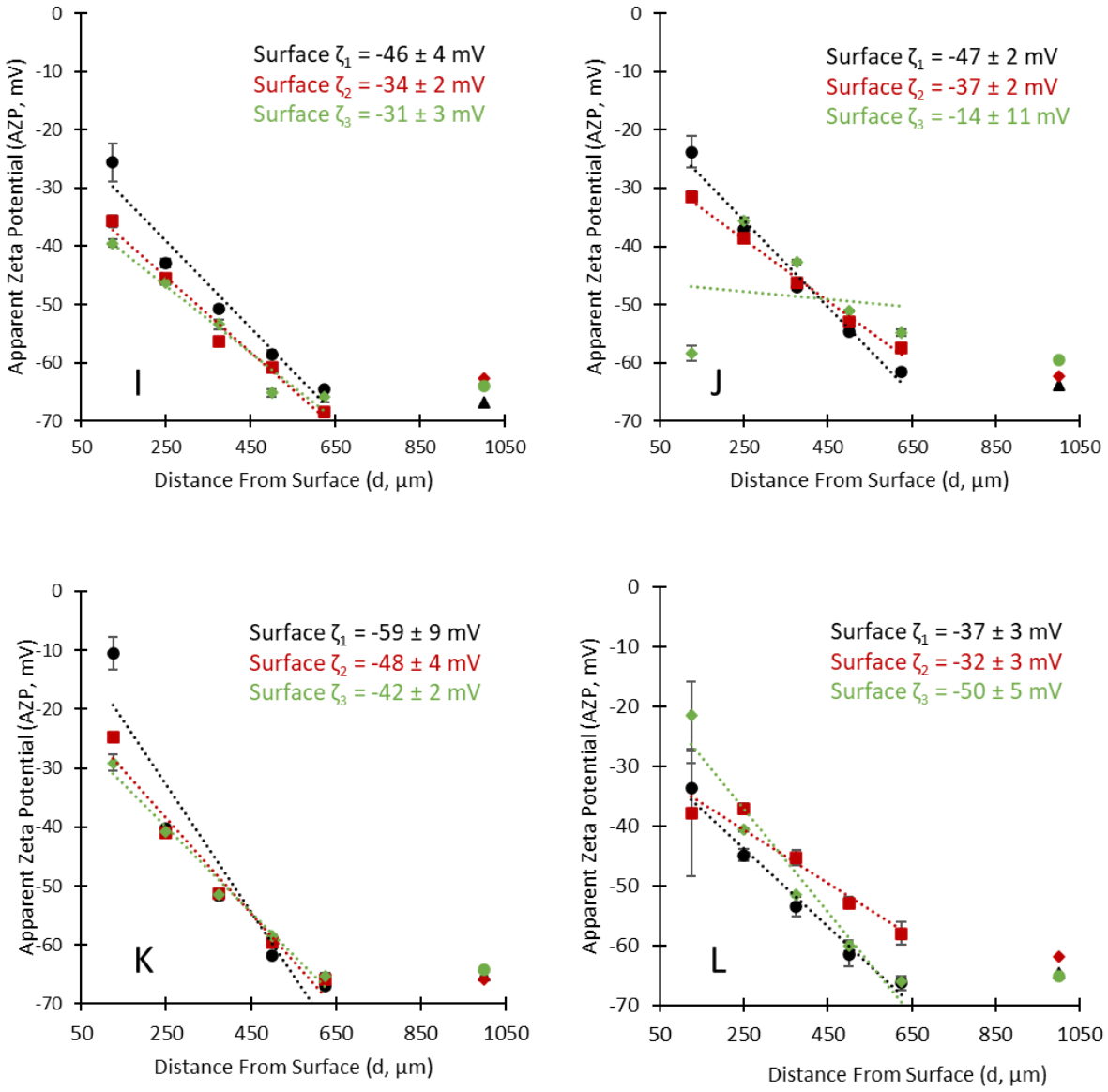

Figure 22. Surface zeta potential measurements of vacuum-evaporated silver films on a Nylon substrate using pH 9.2 silica tracer suspension. In panels I – K, the data for the three separate films are shown, respectively. In Panel L, the average of each sample is shown with, ●, ■, and ◆ representing trial 1, 2 and 3 respectively instead of run 1, 2 and 3 as found in Panel I – K. In each panel, ● (run 1), ■ (run 2), and ◆ (run 3) represent the apparent zeta potential of the tracer particles at the indicated distance from the silver surface, while ▲ (run 1), ◆ (run 2), and ● (run 3) represent the zeta potential of the tracer particles. While the error bars in Panels I – K represent the deviation among the 5 measurements made at each distance indicated, the error bars in Panel L represent the deviation between the data in Panels I – K at the indicated distance.

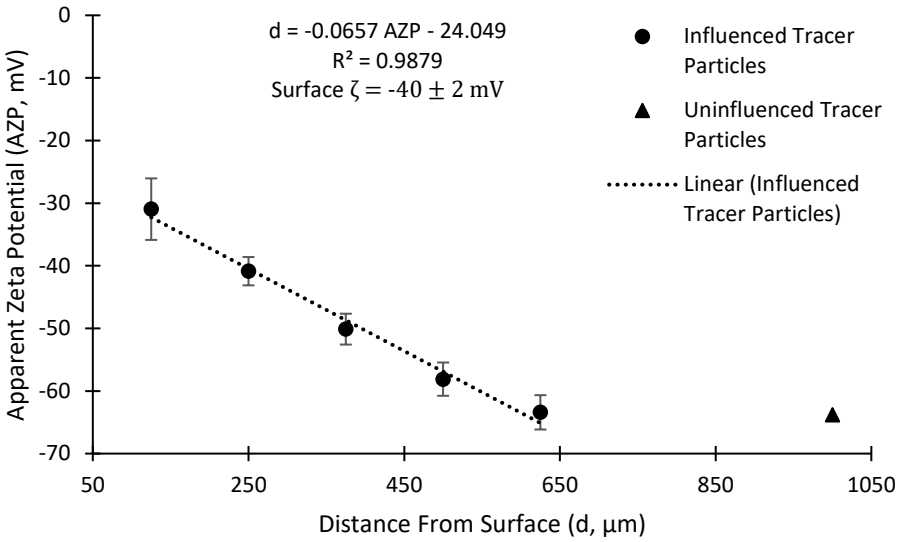

Figure 23. Averaged surface zeta potential measurements of vacuum-evaporated silver films on a Nylon substrate using pH 7 silica nanoparticle tracer suspension.

Table 4. Summary of Linear Regression Analysis and calculated surface zeta potential for each measurement of a silver-coated Nylon substrate exposed to varying pH, as well as the averaged data for each trial (shown in rows D, H and L). Graphical representations of this data are shown in Figure 18-Figure 23.

Sample / Figure Panel	**Run/ Trial**	**Linear Regression Analysis**			**AZP at 1000 µm (mV)**	**Surface Zeta Potential (mV)**
		Slope (mV/µm)	*Intercept (mV)*	*Coefficient of Determ. (R^2)*		
A	1	-0.12	56.7	0.96	-15.9	-73 ± 6
	2	-0.07	27.4	0.99	-15.2	-43 ± 2
	3	-0.05	17.1	0.98	-13.5	-31 ± 2
B	1	-0.06	19.8	0.99	-15.8	-36 ± 2
	2	-0.06	14.4	0.98	-21.3	-36 ± 2
	3	-0.04	1.7	0.99	-20.9	-23 ± 1
C	1	-0.06	24.7	0.98	-12.9	-38 ± 2
	2	-0.05	15.5	0.99	-15.1	-31 ± 1
	3	-0.04	12.6	0.99	-11.5	-24 ± 1
D	1	*-0.08*	*33.7*	*0.98*	*-14.9*	*-49 ± 3*
	2	*-0.05*	*11.9*	*0.99*	*-19.4*	-31 ± 2
	3	*-0.05*	*17.6*	*0.99*	*-13.2*	-31 ± 1
E	1	-0.07	-10.8	0.99	-57.6	-47 ± 2
	2	-0.07	-16.9	0.99	-58.0	-41 ± 2
	3	*-0.11*	*12.1*	*0.96*	*-51.4*	*-63 ± 5*
F	1	-0.06	-27.6	0.96	-59.6	-32 ± 3
	2	-0.10	32.8	0.95	-56.2	-89 ± 5
	3	*-0.10*	*6.0*	*0.95*	*-58.7*	*-65 ± 5*
G	1	-0.05	-31.6	0.99	-62.0	-30 ± 1

	2	-0.09	-15.2	0.94	-61.9	-47 ± 5
	3	*-0.09*	*-15.9*	*0.96*	*-61.6*	*-46 ± 4*
	1	*-0.08*	*-5.2*	*0.98*	*-55.7*	*-50 ± 3*
H	*2*	*-0.09*	*3.7*	*0.99*	*-58.2*	*-62 ± 2*
	3	*-0.07*	*-20.9*	*0.97*	*-61.9*	*-41 ± 3*
	1	-0.08	-20.4	0.95	-66.9	-46 ± 4
I	2	-0.07	-29.1	0.98	-62.8	-34 ± 2
	3	-0.06	-32.5	0.96	-63.9	-31 ± 3
	1	-0.07	-16.9	0.98	-63.7	-47 ± 2
J	2	-0.05	-25.5	0.99	-62.2	-37 ± 2
	3	-0.07	-45.9	0.02	-59.5	-14 ± 11
	1	-0.11	-5.9	0.89	-65.2	-59 ± 9
K	2	-0.08	-182	0.97	-65.8	-48 ± 4
	3	-0.07	-21.9	0.98	-64.2	-42 ± 2
	1	*-0.07*	*-27.3*	*0.98*	*-64.5*	*-37 ± 3*
L	*2*	*-0.05*	*-29.4*	*0.93*	*-61.8*	*-32 ± 3*
	3	*-0.09*	*-15.4*	*0.95*	*-65.1*	*-50 ± 5*

The data presented in Table 4 corresponds to the data presented in Figure 18, Figure 20Figure 22. The rows labeled A – C (cf. Figure 18) indicates the regression analysis information and calculated SZP for each substrate in the pH 5 trial. Similarly, rows E, F, and G correspond to each substrate in the pH 7 trial (cf. Figure 20E – Figure 20G) and rows I, J and K correspond to each substrate in the pH 9.2 trial (cf. Figure 22I – Figure 22K). The row labeled D corresponds to Figure 18D and indicates the average data for substrates A – C where each individual measurements at each measurement position for the three substrates were first averaged together, followed by linear regression analysis and calculation of the SZP. Rows labeled H and L correspond to Figure 20H and Figure 22L, respectively, and indicate the average data for substrates E – G and I – K, respectively. “Run 1” indicates the first SZP measurement, “Run 2” indicates the second SZP measurement on the same substrate and “Run 3” is the third SZP measurement on the same substrate for rows labeled A – C, E – G and I – K. For rows labeled D, H and L; “Run 1” is instead “Trial 1” and indicates that “ Run 1”, “Run 2” and “ Run 3” for the first panel (cf. Figure 18A, Figure 20E and Figure 22I) was averaged to obtain an overall average for that substrate. “Run 2” and “Run 3” for rows labeled D, H and L also

represent “Trial 2” and “ Trial 3”, which were calculated similarly to “Trial 1” but with panel 2 (cf. Figure 18B, Figure 20F and Figure 22J) and panel 3 (cf. Figure 18C, Figure 20G and Figure 22K), respectively. From the data in Table 4, the ZP of the silica tracer particle showed some discrepancy when compared to the initial measurement of the suspensions (cf. section 3.1). The initial ZP of the pH 5 silica suspension was calculated to be -13 ± 0.5 mV, the data for the pH 5 trial in Table 4 has the ZP for the silica particles ranging from -11.5 mV to - 21.3 mV. The pH 7 ZP of the silica tracer suspension also varies from -51.4 mV to -62 mV, when the initial ZP was calculated at -56 ± 3 mV. The ZP range for the pH 9.2 silica particles was from -59.5 mV to -66.9 mV as compared to the initial calculated value of -75 ± 2 mV. The silica particles used were 293 ± 14 nm, so the variance above and below the initial calculated ZP values for pH 5 and pH 7 could be contributed to by the ± 14 nm error in the silica particle size. However, the discrepancy seems to be with the pH 9.2 ZP range as the range is well below the -75 ± 2 mV that was initially calculated. If the variance in the ZP of the pH 9.2 silica particles was due to the ± 14 nm error in the particle size, then the variance should fall on both the upper and lower side of that value instead of the range not including the value at all. Discrepancies in the trend of the ZP of the particles at 1000 μm is important as that value is used along with the intercept of the regression line to calculate the SZP (cf. Equation 6).

A comparison of the pH 9.2 silica trial and the silver coated nylon substrate runs trial (cf. Table 3) was conducted to see how the SZP value calculated using the silica tracer solution compared to that obtained with the zeta potential transfer standard provided by Malvern. The SZP of the pH 9.2 silica trial ranged from -14 ± 11 mV to -59 ± 9 mV, however, with an R^2 value of 0.02 the -14 ± 11 mV is a clear outlier making the range -31 ± 3 mV to -59 ± 9 mV. The average SZP for the pH 9.2 silica trial was -40 ± 2 mV. The SZP values for the silver coated

nylon substrate runs trial ranged from -26 mV to -71 mV and the average SZP of the trial as a whole was -40 ± 13 mV. So, while the range of SZP between the two trials is different, with the larger trial (runs trial) containing the range of the smaller trial (silica pH 9.2), the averaged SZP of the two trials were within error of each other. This shows that the silica suspension used in the pH 9.2 silica trial was able to produce similar results to those produced by the zeta potential transfer standard provided by Malvern.

The silica 9.2 pH data was then compared to the sliver coated nylon substrate 3-runs trial in order to see if the silica data followed the same trend found in section 3.5. The 3-runs trial was chosen over the whole data set as it had the same number of runs and sample size as the silica pH 9.2 data while still representing the trend present in the data as a whole. First an F-test for variance was performed to determine which t-test to use, this resulted in an F critical value of 3.438 and an F-value of 1.792. Since the F value was less than the F critical value then the two sets of data have equal variance and a t-test assuming equal variance can be used. The t-test produced a t value of -0.0208 which was less than the t critical value for two tails of 2.1199 and the P value is greater than 0.05 at 0.9836 meaning that there is no statistical difference between the two sets of SZP data. Therefore, it can be concluded that the silica pH 9.2 SZP data does indeed follow the trend set by the silver coated nylon 3-runs trial. The silica pH 5 and pH 7 SZP data was then compared to the silica pH 9.2 SZP data in order to see if they also followed the trend. The silica pH 5 SZP data was tested for variance with an F value of 0.7426 which was greater than the F critical value of 0.2909 meaning that there is unequal variance when comparing the pH 5 data to the pH 9.2 data. Using a t-test for unequal variance the silica pH 5 and pH 9.2 data were compared, resulting in a t value of -0.3902 which was less than the t critical value of 2.1199 and had a P value greater than 0.05 at 0.3507 meaning that there is no

statistical difference between the two data sets. The silica pH 7 data had an F value of 0.4796 which was greater than the F critical value of 0.2908 meaning it has unequal variance with the pH 9.2 SZP data. Therefore, a t-test assuming unequal variance was used resulting in a t stat of 1.5095 which was less than the t critical value of 2.1447 and had a P value greater than 0.05 at 0.1534 meaning that the SZP data between the silica pH 7 and pH 9.2 are not statistically different. Therefore, the silica pH 5 and pH 7 SZP data follows the same trend as the silica pH 9.2 SZP data.

As a measurement of the pH dependency of SZP, this data is insufficient. For the pH dependence of SZP to be properly determined, the range of pH values tested would need to be increased as well as the isoelectric point identified for the silica particles used. The plain nylon should also be tested across the same pH range to determine if the presence of silver is influencing that measurement and to provide a reference point, using this technique, for comparison with pH 5 and pH 7 silica data. With those adjustments and the adjustments to the measurement method discussed in section 3.5, a true measure of the pH dependence of SZP could be determined.

3.8 ICP-OES Results for Silver Coated Substrate Runs Trial

With the surface seeming to be undergoing rearrangement during the measurement process, it was important to determine whether multiple runs affected the rearrangement of the surface. This was done according to the procedure in section 2.2.3 and analyzed using statistical analysis. Since silver emits most of its light at 328.1 nm when ionized and excited, the data analyzed for the mass of silver on the substrates was at 328.068 nm wavelength. The averages masses of silver and standard deviation for each of the samples are shown in Table 5. Each of the wet control samples only had one measurement at the 328.068 nm wavelength and therefore had

a standard deviation of zero, which was an oversight as each other sample was measured in triplicate.

Table 5. 328.068 nm wavelength ICP-OES average mass of silver per sample.

Sample	Average mass of silver (µg)	Standard Deviation (µg)
Dry control	4.62	± 0.43
1 run wet control	4.34	± 0
2 run wet control	5.07	± 0
3 run wet control	4.67	± 0
1 run	3.00	± 0.13
2 runs	3.41	± 0.36
3 runs	3.04	± 0.55

From the average mass of silver per sample, the run samples all have less silver present than both the wet and dry controls. This supports the hypothesis that the process of performing zeta measurements on a sample does affect the surface, specifically causing a rearrangement of the surface. The question of whether the number of runs influences the surface rearrangement is not as clear and as such two, single factor ANOVA tests were performed. The first single factor ANOVA was performed to determine if there is a significant difference between the sample groups. The first ANOVA test resulted in a P-value of 6.82×10^{-8} with an F value of 17.52 and an F critical value of 2.65; since the P-value is less than 0.05 and the F value is greater that the F critical value there is a significant difference between sample groups. The second ANOVA test was performed in order to rule out the significant difference being between the three run samples. The second test resulted in a P-value of 0.316 and an F value of 1.208 and an F critical value of 3.403; the P-value being greater than 0.05 and the F-value being less than the F critical

value means that there is not a significant difference between the three run sample data. This necessitated doing partwise t-tests between the remaining samples, but first a two-sample F-test for variance is needed to determine whether the t-test should assume equal variance or unequal variance. The first F-test between the dry and wet control had an F-value of 2.672 and an F critical value of 19.371. Since the F-value is less than the F critical value then the variance between the dry and wet control is equal. This was repeated for the rest of the samples and all the results can be seen in

Table 6.

Table 6. Two-sample F-test for variance data.

Samples compared	F-value	F critical value	Equal or unequal variance?
Wet and dry control	2.672	19.37	Equal
Dry control and run 1	1.134	3.438	Equal
Dry control and run 2	5.194	3.438	Unequal
Dry control and run 3	1.440	3.438	Equal

With the F-Values of all dry control and run sample couplings, except dry control and run 2, being less than the F critical value of 3.438 all the variances were determined. These variances were then used to perform the two-sample t-tests with the results being displayed in Table 7.

Table 7. Two-sample t-test result.

Samples compared	Two tail P-value	Greater than 0.05?	Significantly different?
Wet and dry control	0.1625	Yes	No
Dry control and run 1	2.18×10^{-8}	No	Yes
Dry control and run 2	0.0013	No	Yes

Dry control and run 3	1.2×10^{-7}	No	Yes

The first ANOVA test results showed that there is a significant difference between the sample groups. The second ANOVA test results showed that there was no significant difference between the three run samples and confirms that the number of runs does not statistically affect the surface. When the ANOVA results are combined with the t-test results, it also shows that the dry and wet controls are not significantly different from each other but are significantly different from the runs.

3.9 Scanning Electron Microscopy Results

In order to understand the effect that the SZP measurement process was having on the silver nanoparticle surface, scanning electron microscopy (SEM) was used to observe the surface. One silver coated substrate that had not undergone the SZP measurement was observed as a control and a sample substrate that had undergone the SZP measurement was observed for comparison.

A)

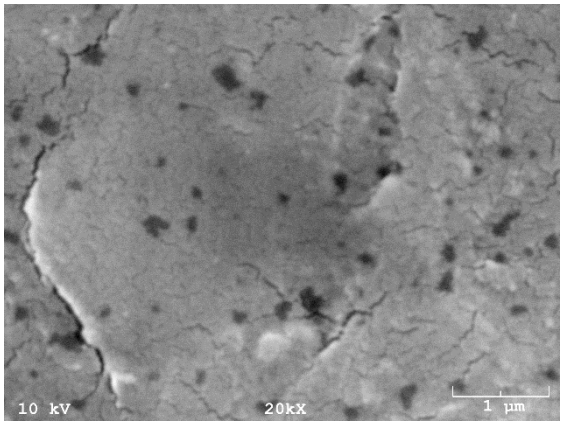

B)

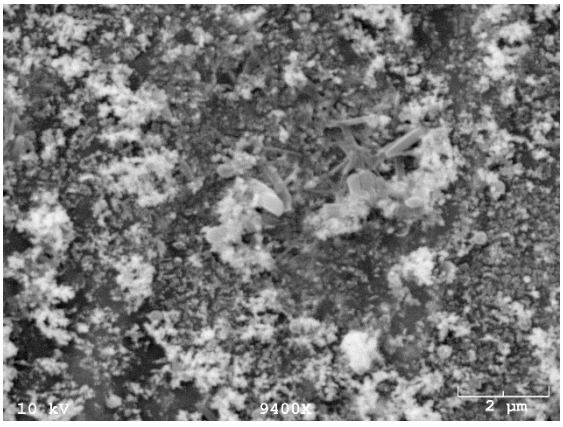

Figure 24. A) SEM image of the silvered surface of a nylon substrate used as a control. B) SEM image of the silvered surface of a nylon substrate after undergoing the SZP measurement process.

As seen in Figure 24 A, the control substrate had a fully percolated silver surface with some pinholes that seem to extend to the nylon substrate. Given that the deposition thickness was only 35 nm, this high degree of percolation was unexpected. The substrate exposed to the SZP measurement procedure on the other hand, as seen in Figure 24 B, showed significant rearrangement of the surface with a much more heterogeneous distribution of silver. This rearrangement could be a result of an 'electrochemical interaction' during the SZP measurement process or a physical interaction of the tracer particles and the silver surface. During the SZP measurement the tracer particles are rapidly shuttled parallel to the silver surface. It is possible that the tracer particles in very close proximity to the silver abrade the surface resulting in rougher features and could explain the presence of silver in the tracer suspension (cf. section 3.8). With respect to the possibility of an electrochemical interaction, the SZP measurement procedure, which involves placing the silver surface within the electric field of two parallel plate electrodes, is somewhat reminiscent of the standard practice of electrochemical roughening of silver substrates for SERS spectroscopy.[25] For example a paper by Tuschel, *et al.*, shows an electrochemical way to roughen an Ag electrode using an oxidation-reduction cycle (ORC). The Ag electrode was placing in an aqueous media containing chloride (Cl^-). The Cl^- ions when influenced by an electrical potential will oxidize the Ag surface to form AgCl. The newly formed AgCl will then be reduced and redeposited when the direction of the potential is reversed.[25] This ORC environment is similar to the environment the silver coated nylon substrate is exposed to as the tracer particle suspension used on the two samples in Figure 24 contained Cl^- ions. Unlike in electrochemical roughening, the silver film in the SZP measurements is not an electrode.

However, during the measurement the chemical environment is similar and could result in a similar interaction in which redox chemistry affects the surface structure and leads to the formation of AgCl in the tracer particle suspension. Although the experiments in section 3.3 did not seem to indicate a change in the silver surface, it is possible that the electric field produced during the measurement affected that interaction. However, no tests were done to confirm if the rearrangement of the silver surface was caused by physical abrasion of tracer particles or an electrochemical ORC of the Ag with the Cl^- ions due to time constraints.

The SEM images caused more questions than answers when it comes to understanding what is happening to the surface over the course of the SZP measurements. Since access to SEM was not readily available, only one control sample and one test sample were sent for analysis. This limited data brings up the question of when the rearrangement is occurring. If the rearrangement is occurring on the first displacement as was previously thought, then the SZP data obtained throughout this research would represent the final surface. However, if the rearrangement occurs gradually throughout the process, then the SZP data at each displacement is only representative of brief snapshot of a changing surface and not the final surface. The second case could explain some of the variance seen in the data shown in previous figures. If access to SEM had of been available and these results seen sooner, then a simple experiment could have been performed to determine if the surface was being continuously rearranged during the SZP measurement process. This could be accomplished by having a sample that corresponds to each of the 6 electrode cycles undergo SEM imaging before the SZP measurement and then once more after each cycle until the last cycle for that sample was reached. The images could then be compared to see if the rearrangement is only occurring at the first cycle, if it continues until the last cycle or continuously throughout the measurement. This experiment could then be

repeated in which the particles are removed from the tracer suspension, leaving only the electrolyte solution which contains chloride. Similar results from the two trials would indicate that electrochemical interaction is causing the change in the surface roughness, while no change in the silver surface after the second trial would indicate that the physical interaction between the tracer particles and the silver surface is causing the change in the surface roughness.

CHAPTER 4. CONCLUSION AND FUTURE WORK

Using the dip cell arrangement proposed by Corbett, *et al.,* and following the method outlined in section 2.4.2 quantifiable data for the determination of the SZP of silver coated nylon substrates was obtained. This method also allowed for the determination of SZP of silver coated nylon substrates at the desired pH values of 5, 7 and 9.2. It was found, through statistical analysis, that the measurement process itself has variance that can be seen in the intercepts of the linear regressions but that it does not affect the overall trend of the data as indicated by the lack of statistical difference in the slope. It was also determined through ICP-OES analysis of samples exposed to varying number of runs that the surface is losing silver to solution but that the number of runs does not seem to directly relate to the amount of silver lost. SEM imaging confirmed that the silver surface of the substrate is undergoing rearrangement, but statistical analysis showed that the rearrangement does not have a statistically significant impact on the measurements.

This project shows that the SZP of a silver coated substrate can be determined from the data obtained from the method presented, however, there is more that needs to be done to expand and standardize this method. The first way the method needs to be expanded on is the sample preparation. All the silver samples used in this project were 350 angstroms thick (35 nm) with a deposition rate of 1 angstrom per second. Investigating different surface thicknesses and deposition rates could provide an optimized way to prepare the sample to minimize the effects of surface disparities. The method itself can also be refined with further testing, such as changing the delay between runs, changing the equilibration time and investigating how the mechanism for the surface rearrangement as well as whether the rearrangement is ongoing during the measurement or simply at the beginning of the measurement. Using this method once the sample preparation and measurement protocol is standardized to reduce the sources of error, then an

experiment of interest would be to take a batch of samples and determine a standard value for the SZP of silver on a nylon substrate with this method. This is an experiment that was planned, but due to time restraints was not performed. The tracer particle ZP across the project for the experiments using the Malvern particles varied from -39 to -48 mV for the silver coated trials and -47 ± 4 mV which are relatively close to the -42 ± 4.2 mV reported by Malvern. In order to see the effect, the Ag^+ lost to solution from the silver coated substrates has on the ZP of the tracer particles by redoing the nylon trial runs while titrating $AgNO_3$ to introduce Ag^+ into the solution for comparison to the silver coated trials. A similar model to Equation (5) from the Morga, *et al.,* paper for the substrate in this research would allow for the calculation of the ZP of the substrate with respect to the coverage of silver on the substrate and EDL thickness allowing for a better understanding of the ZP and surface chemistry.[11] With a better understanding of the ZP of a surface comes a better understanding of how molecules interact with that surface. Understanding these interactions would allow for optimizations with respect to surface chemistry. This project has set the foundation for further study of SZP of silver coated nylon substrates to eventually understand how human bodily fluids will interact with the silver coated nylon evidence swabs being developed by the Evanoff research group. This understanding will hopefully allow for the optimization of the SERS analysis of human bodily fluids and the development of a one-step non-destructive method for analyzing human bodily fluids found in sexual assault cases.

WORKS CITED

(1) Corbett, J. C. W.; Mcneil-watson, F.; Jack, R. O.; Howarth, M. Colloids and Surfaces A : Physicochemical and Engineering Aspects Measuring Surface Zeta Potential Using Phase Analysis Light Scattering in a Simple Dip Cell Arrangement. *Colloids and Surfaces A: Physicochemical and Engineering Aspects* **2012**, *396*, 169–176. https://doi.org/10.1016/j.colsurfa.2011.12.065.

(2) Bhattacharjee, S. DLS and Zeta Potential - What They Are and What They Are Not? *Journal of Controlled Release* **2016**, *235*, 337–351. https://doi.org/10.1016/j.jconrel.2016.06.017.

(3) Bajpai, P. Colloid and Surface Chemistry. In *Biermann's Handbook of Pulp and Paper*; Elsevier, 2018; pp 381–400. https://doi.org/10.1016/b978-0-12-814238-7.00019-2.

(4) Kaszuba, M.; Corbett, J.; Watson, F. M. N.; Jones, A. High-Concentration Zeta Potential Measurements Using Light-Scattering Techniques. *Philosophical Transactions of the Royal Society A: Mathematical, Physical and Engineering Sciences* **2010**, *368* (1927), 4439–4451. https://doi.org/10.1098/rsta.2010.0175.

(5) O'brien, R. W.; Cannon, D. W.; Rowlands, W. N. Electroacoustic Determination of Particle Size and Zeta Potential. *Journal of Colloid And Interface Science*. 1995, pp 406–418. https://doi.org/10.1006/jcis.1995.1341.

(6) Peeters, J. M. M.; Mulder, M. H. V.; Strathmann, H. Streaming Potential Measurements as a Characterization Method for Nanofiltration Membranes. *Colloids and Surfaces A: Physicochemical and Engineering Aspects* **1999**, *150* (1–3), 247–259. https://doi.org/10.1016/S0927-7757(98)00828-0.

(7) Lee, T. T.; Dadoo, R.; Zare, R. N. Real-Time Measurement of Electroosmotic Flow in Capillary Zone Electrophoresis. *Analytical Chemistry* **1994**, *66* (17), 2694–2700. https://doi.org/10.1021/ac00089a016.

(8) Vasconcelos, J. M.; Zen, F.; Stamatin, S. N.; Behan, J. A.; Colavita, P. E. Determination of Surface ζ-Potential and Isoelectric Point of Carbon Surfaces Using Tracer Particle Suspensions. *Surface and Interface Analysis* **2017**, *49* (8), 781–787. https://doi.org/10.1002/sia.6223.

(9) Sun, D.; Kang, S.; Liu, C.; Lu, Q.; Cui, L.; Hu, B. Effect of Zeta Potential and Particle Size on the Stability of SiO2 Nanospheres as Carrier for Ultrasound Imaging Contrast Agents. *International Journal of Electrochemical Science* **2016**, *11* (10), 8520–8529. https://doi.org/10.20964/2016.10.30.

(10) He, C.; Xie, F. Adsorption Behavior of Manganese Dioxide Towards Heavy Metal Ions: Surface Zeta Potential Effect. *Water, Air, and Soil Pollution* **2018**, *229* (3). https://doi.org/10.1007/s11270-018-3712-6.

(11) Morga, M.; Adamczyk, Z.; Oćwieja, M. Stability of Silver Nanoparticle Monolayers Determined by in Situ Streaming Potential Measurements. *Journal of Nanoparticle Research* **2013**, *15* (11). https://doi.org/10.1007/s11051-013-2076-5.

(12) Edwards, H. G. M. *Modern Raman Spectroscopy—a Practical Approach.Ewen Smith and Geoffrey Dent. John Wiley and Sons Ltd, Chichester, 2005. Pp. 210. ISBN 0 471 49668 5 (Cloth, Hb); 0 471 49794 0 (Pbk)*; 2005; Vol. 36. https://doi.org/10.1002/jrs.1320.

(13) Hao, J.; Han, M.; Han, S.; Meng, X.; Su, T.; Wang, Q. K. ScienceDirect Invited Article SERS Detection of Arsenic in Water : A Review. *JES* **2015**, *36* (V), 152–162. https://doi.org/10.1016/j.jes.2015.05.013.

(14) Stefancu, A.; Moisoiu, V.; Couti, R.; Andras, I.; Rahota, R. Combining SERS Analysis of Serum with PSA Levels for Improving the Detection of Prostate Cancer. **2018**, *13*, 2455–2467.

(15) Burleson, M. SERS-Active Nylon Fiber Evidence Swabs for Forensic Applications, Western Carolina University, 2016.

(16) Perrine, K. OPTIMIZATION OF THE FABRICATION PARAMETERS FOR SERS-ACTIVE FORENSIC EVIDENCE SWABS, Western Carolina University, 2018.

(17) Alvarez-Puebla, R. A.; Arceo, E.; Goulet, P. J. G.; Garrido, J. J.; Aroca, R. F. Role of Nanoparticle Surface Charge in Surface-Enhanced Raman Scattering. *Journal of Physical Chemistry B* **2005**, *109* (9), 3787–3792. https://doi.org/10.1021/jp045015o.

(18) Evanoff, D. D.; Chumanov, G. Size-Controlled Synthesis of Nanoparticles. 1. "Silver-Only" Aqueous Suspensions via Hydrogen Reduction. *Journal of Physical Chemistry B* **2004**, *108* (37), 13948–13956. https://doi.org/10.1021/jp047565s.

(19) Oh, M.-H.; So, J.-H.; Lee, J.-D.; Yang, S.-M. Preparation of Silica Dispersions and Its Phase Stability in the Prescence of Salts. *Korean J. Chem. Eng.* **1999**, *16* (4), 532–537.

(20) Shi, Y. R.; Ye, M. P.; Du, L. C.; Weng, Y. X. Experimental Determination of Particle Size-Dependent Surface Charge Density for Silica Nanospheres. *Journal of Physical Chemistry C* **2018**, *122* (41), 23764–23771. https://doi.org/10.1021/acs.jpcc.8b07566.

(21) Ripoll, L.; Bordes, C.; Marote, P.; Etheve, S.; Elaissari, A.; Fessi, H. Electrokinetic Properties of Bare or Nanoparticle-Functionalized Textile Fabrics. *Colloids and Surfaces A: Physicochemical and Engineering Aspects* **2012**, *397* (March), 24–32. https://doi.org/10.1016/j.colsurfa.2012.01.022.

(22) Yaqoob, S. B.; Adnan, R.; Rameez Khan, R. M.; Rashid, M. Gold, Silver, and Palladium Nanoparticles: A Chemical Tool for Biomedical Applications. *Frontiers in Chemistry* **2020**, *8* (June), 1–15. https://doi.org/10.3389/fchem.2020.00376.

(23) Evanoff, D. D.; White, R. L.; Chumanov, G. Measuring the Distance Dependence of the Local Electromagnetic Field from Silver Nanoparticles. *Journal of Physical Chemistry B* **2004**, *108* (5), 1522–1524. https://doi.org/10.1021/jp036899z.

(24) Kinnan, M. K.; Chumanov, G. Plasmon Coupling in Two-Dimensional Arrays of Silver Nanoparticles: II. Effect of the Particle Size and Interparticle Distance. *Journal of Physical Chemistry C* **2010**, *114* (16), 7496–7501. https://doi.org/10.1021/jp911411x.

(25) Tuschel, D. D.; Pemberton, J. E.; Cook, J. E. SERS and SEM of Roughened Silver Electrode Surfaces Formed by Controlled Oxidation-Reduction in Aqueous Chloride Media. *Langmuir* **1986**, *2* (4), 380–388. https://doi.org/10.1021/la00070a002.